Ocean Engineering 290 (2023) 116221

Contents lists available at ScienceDirect

Ocean Engineering

journal homepage: www.elsevier.com/locate/oceaneng

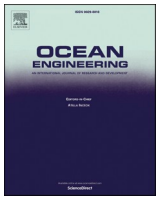

Experiments on flow-induced vibration of four flexible cylinders with large aspect ratio in a square configuration

Yexuan Ma [a], Zhiyou Song [b], Jingyu Xu [a], Wanhai Xu [b,*]

[a] Institute of Mechanics, Chinese Academy of Sciences, Beijing, 100190, China
[b] State Key Laboratory of Hydraulic Engineering Simulation and Safety, Tianjin University, Tianjin, 300350, China

ARTICLE INFO

Handling Editor: Prof. A.I. Incecik

Keywords:
Flexible cylinder
Square configuration
Flow-induced vibrations
Incidence angle
Multi-mode

ABSTRACT

A system consisting of four cylinders positioned in the quadrilateral arrangement represents the prevalent and fundamental constituent within pipe bundles and tube banks in numerous engineering scenarios. This research presents a laboratorial study on flow-induced vibration (FIV) exhibited by four flexible cylinders positioned within a square geometric arrangement. The uniform flows were produced by a carriage on the top of a towing tank. Considering flow velocities and structural parameters, Reynolds number could reach 16000. The spacing between the cylindrical centres was selected as 6.0 D (D denotes the outer diameter of cylinders), and two typical incidence angles 0° and 45° were examined. For each flexible cylinder model, strain gages at seven distinct measuring positions were utilized to collect the oscillation data in cross-flow (CF) and in-line (IL) directions. Principal vibration modes, response frequencies, response amplitudes and motion trajectories were presented to understand the FIV features. For incidence angles 0°, considering the four flexible cylinders as two sets of tandem cylinders arranged in parallel is not appropriate due to the proximate effect. The behaviours of the two upstream cylinders resembles those of the pair of cylinders positioned in a side-by-side configuration, whereas behaviours for the downstream cylinders are influenced by wake interference generated from leading cylinders. IL response frequencies decrease to the values close to the CF response frequencies, resulting in the elliptical-shaped motion trajectories with large IL displacements. For incidence angles 45°, the upstream cylinder displays characteristics akin to those of a solitary cylinder experiencing vortex-induced vibration (VIV). Reactions for the central pair of cylinders result from the amalgamation of VIV and wake-induced flutter. While, reactions observed for downstream cylinder are characterized by low frequencies, significant IL displacements and more chaotic trajectories.

1. Introduction

Flow past cylindrical structure systems, such as mooring lines, marine risers, subsea pipelines and etc., will lead to vibration that is called flow-induced vibration (FIV). The fatigue-related damage resulted from FIV has prompted widespread concern in numerous engineering fields, which makes it essential to understand the FIV dynamic characteristics. The cylindrical structure system usually consists of multiple cylinders arranged in various configuration. The oscillations emanating from neighbouring cylinders will engage in mutual interaction through the wake flows, thereby enhancing the complexity of FIV. For the last few decades, extensive research efforts have been dedicated to investigating wake patterns, responses features and mutual interactions of multiple cylinders undergoing FIV (Alam et al., 2003; Bearman and Wadcock, 1973; Khan et al., 2022; Kim and Alam, 2015; Nguyen et al., 2018; Sumner, 2010; Wang et al., 2019; Wu, 2017; Zdravkovich, 1987).

The two cylinders are always considered as a prevalent and fundamental constituent within a cylindrical structure system. The wake patterns behind a pair of cylinders under the oncoming flow have attracted much attention in the beginning (Zdravkovich, 1985). Various wake patterns of two cylinders will be observed contingent upon the arrangement and spacing ratio P/D (P represents the interval between the cylindrical centres, and D represents the outer diameter). In the configuration where cylinders are placed side-by-side, the wake patterns are influenced by the proximate effect. A pair of vortex streets type, wide-narrow wake type and two pairs of vortex streets type gradually would appear with the increasing P/D (Sumner, 2010; Williamson, 1985). For the tandem arrangement, it is essential to study the behaviours of shear layers. Various wake types can be gradually observed with increasing P/D, namely, shear layers wrapping downstream cylinder,

* Corresponding author.
E-mail address: xuwanhai@tju.edu.cn (W. Xu).

https://doi.org/10.1016/j.oceaneng.2023.116221
Received 25 August 2023; Received in revised form 16 October 2023; Accepted 29 October 2023
Available online 24 November 2023

shear layers reattaching downstream cylinder, and vortex regenerating types (Sumner, 2010; Zdravkovich, 1987). The flow patterns encompassing two staggered cylinders are significantly impacted by both *P/D* and incidence angle. Totally nine types of wake pattern are recognized, demonstrating the considerably greater complexity in the flow characteristics of two staggered cylinders (Sumner et al., 2000).

Unlike a solitary cylinder, response characteristics observed for two cylinders exhibit noteworthy distinctions owing to their mutual interaction. Two rigid cylinders supported with elasticity and positioned side-by-side would vibrate together at a half frequency of a solitary cylinder when *P/D* is small. As *P/D* increases, the narrow wake and wide wake appear. Consequently, the cylinder experiencing a narrow wake pattern exhibits greater response amplitude and frequency compared to the cylinder subjected to a wide wake pattern. Once the two sets of coupled vortex patterns emerge, vibration characteristics of the pair of cylinders become comparable (Chen et al., 2015, 2022; Xu et al., 2022a). For a pair of cylinders positioned in a tandem configuration, the downstream cylinder could disturb flows coming from the upstream direction at small and intermediate *P/D*, resulting in distinct responses patterns for both cylinders. Once *P/D* reaches a sufficient magnitude for complete vortex maturation, the upstream cylinder resembles a solitary cylinder undergoing vortex induced vibration (VIV). Meanwhile, vibration amplitude of the downstream cylinder notably escalates as a result of impacts from vortices generated upstream. (Assi et al., 2010; Haider and Sohn, 2022; Kim et al., 2009; Mousavisani et al., 2022; Narváez et al., 2020; Wang et al., 2017; Xu et al., 2019, 2021a). In staggered configurations, the FIV features predominantly contingent upon the spacing ratios and incidence angles. With a small *P/D*, the flow passing through the narrow gap can induce substantial amplitude oscillations in both cylinders when the incidence angle is below 15°, while the two cylinders behave small amplitude vibrations as the increase of incidence angle (Alam and Kim, 2009; Griffith et al., 2017). With an intermediate *P/D*, oscillations of the upstream cylinder are mitigated owing to these incompletely developed downstream vortices when the incidence angle is below 15° (Xu et al., 2022b). As the *P/D* increases, the phenomenon of wake-induced flutter (WIF), characterized by a noteworthy rise in IL vibration amplitude, becomes apparent for the downstream cylinder. (Assi, 2014; Fukushima et al., 2021; Prasanth and Mittal, 2009). The elliptical shape motion trajectory is observed owing to the comparable vibration frequency in the two directions (Huang and Herfjord, 2013; Xu et al., 2020). The FIV features of two flexible cylinders are more complex. For a pair of side-by-side flexible cylinders, the threshold value of *P/D* at which the proximity effect appears is higher than that of two rigid cylinders with elastic support (Sanaati and Kato, 2014; Xu et al., 2022). The proximity effect amplifies in-line (IL) oscillations even as *P/D* is increased to 8.0 (Xu et al., 2018a). For a pair of tandem flexible cylinders, the continuous increase in the oscillation amplitude disappears in FIV of downstream flexible cylinders due to the occurrence of the high order mode vibrations (Huera-Huarte and Bearman, 2011; Xu et al., 2018b). Lin et al. (2021) carried out a numerical simulation on FIV of two tandem flexible cylinders and better revealed the interaction between the two cylinders. The influence of the upstream wake interference acting on the downstream cylinder reduced when the upstream vortex impinged on the downstream cylinder, and the influence enhanced as the downstream cylinder entered the gap between the upstream vortices.

The mutual interaction between the two-cylinder system may represent some basic mechanisms of interference among multiple cylinders. However, there are still some typical phenomena that are not observed in the two-cylinder system. Some researchers have studied the wake interference of a three-cylinder system (Bansal and Yarusevych, 2017; Gu and Sun, 2001; Kareem et al., 1998; Ma et al., 2019; Pouryoussefi et al., 2009; Sayers, 1987, 1990; Wang et al., 2013; Xu et al., 2014; Yang et al., 2020; Zheng et al., 2016; Xu et al., 2021c). Tatsuno et al. (1998) conducted an experimental exploration of wake patterns involving a group of cylinders positioned in triangular configuration. The distinctive deflective wake pattern was noted for two downstream cylinders. In contrast, the orientation of this deflective wake remained consistent, unlike the intermittent changes observed in a configuration of side-by-side. Gu and Sun (2001) identified seven wake patterns for three equilateral-triangular arrangement cylinders various spacing ratios and incidence angles. Seven wake patterns can be attributed to three kinds of mutual effects. Yang et al. (2020) discovered that the wake interaction generating from a group of three cylinders exhibited certain resemblances to that observed with two cylinders. However, the inclusion of the third cylinder introduced various flow patterns contingent upon factors like *P/D* and incidence angle. In a study conducted by Wang et al. (2013), FIVs of a set of rigid cylinders supported by elasticity and positioned triangular were presented by a numerical simulation. Towards the conclusion of resonance region, Strouhal number for three cylinders exhibited a minor reduction compared to that of a solitary cylinder. As the upstream vortices traversed through the insides of the downstream cylinders, their interaction with internal shear layers generating from the leading cylinders made downstream cylinders have large oscillation amplitude in IL direction and move along an elliptical shape motion trajectory. Xu et al. (2014) declared that downstream cylinders within three equilateral-triangular arrangement cylinders oscillated following elliptical orbits, meaning that the response frequency in cross-flow (CF) direction matched the frequency in IL direction. Meanwhile, oscillation amplitudes were magnified under the influence of the upstream wake flows. Ma et al. (2019) carried out model tests on FIV characteristics of a group of flexible cylinders positioned in a triangular configuration. The downstream cylinder demonstrated significantly heightened oscillation amplitudes in IL direction, showing an enhancement of more than 30% in comparison with a solitary cylinder. In IL displacement spectrograms of downstream cylinder, two distinct frequencies stood out prominently. The high-frequency component approximated principal frequency in IL direction of a solitary cylinder, while the low-frequency component closely matched principal frequency in CF direction. These low-frequency components influenced the downstream cylinder's motion trajectory, deviating it from the typical figure-eight, crescent, and C-shaped patterns commonly observed for a solitary cylinder subjected to VIV.

Several researchers have delved into the investigation of flow pattern and oscillation characteristics of a group of cylinders arranged in the quadrilateral configuration (Gao et al., 2019; Han et al., 2013; Lam et al., 2003a, 2003b; Lam and Fang, 1995; Lam and Lo, 1992; Tu et al., 2020). Fig. 1 provides a schematic representation of four

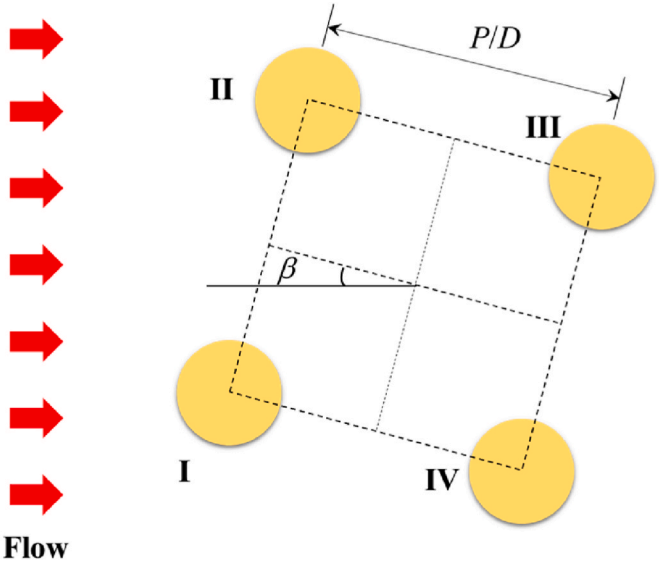

Fig. 1. Illustration of four cylinders arranged in the quadrilateral configuration.

quadrilateral-arranged cylinders, with distinct labels of I, II, III, and IV assigned to each cylinder. Lam and Lo (1992) conducted an investigation into the flow pass through four stationary cylinders in a quadrilateral arrangement. Under an incidence angle of 0°, the configuration of the four cylinders could be approximated as two pair of identical tandem cylinders when P/D surpassed 3.94, primarily owing to the limited influence of the proximity effect. With a more pronounced reduction in P/D, the downstream cylinders inhibited the upstream vortices and a deflective gap flow was observed. As for $0° < \beta < 45°$, the gap flow was much more easily deflective to cylinder IV, consequently leading to the broad flow region around cylinder III. Under an incidence angle of 45°, the flow region around cylinder I was narrow and short due to the gap flow between cylinder I and cylinder II or cylinder IV. The wake flows of cylinders II and IV were biased to the outsides, which caused a wide wake flow of cylinder III. Han et al. (2013) observed that the deflective flow region encompassing cylinders III and IV would disturb the shedding of vortices at $P/D = 1.6$ and $\beta = 0°$. As P/D progressively enlarged, the deflective wake flow disappeared and gave way to two pairs of antisymmetric vortex streets, which resembled the flow region encompassing two side-by-side cylinders. At $\beta = 45°$ and $P/D \leq 2.0$, four cylinders could be perceived as a single bluff body, exhibiting two rows of irregular vortex. However, as P/D climbed to 3.0, the vortices generated by cylinder II and cylinder IV started to intermingle with those produced by cylinder III, which made the vortex shedding more disordered. All the four cylinders could generate vortices and the wake flow became regular again with P/D exceeding 3.5. The vortices originating from cylinder III exhibited an inclination to those generated by cylinder II and cylinder IV. As a consequence, the wake flows of cylinder II and cylinder IV displayed an outward bias, resulting in the wide wake behind cylinder III. Gao et al. (2019) carried out a numerical simulation focusing on four quadrilateral-arranged rigid cylinders with elastic support. Under an incidence angle of 0°, motion trajectories of figure-eight shape appeared for upstream cylinders I and II. While, downstream cylinders III and IV exhibited motion trajectories with elliptical shape characterized by substantial displacements in two directions. Under an incidence angle of 45°, cylinders II, III and IV experience large vibration amplitudes owing to the upstream wake interference. The vortex behind cylinder III was suppressed and the motion trajectory was disordered at low velocity. The vortices from cylinder III were developed as the increasing velocity, which caused a motion trajectory with tear shape.

Nevertheless, research regarding the FIV characteristics of flexible cylinders positioned within a square geometric arrangement remains scarce. Based on the findings from FIV analysis of multiple flexible cylinders, it becomes evident that multiple mode vibrations of flexible cylinders differ significantly from the reaction observed in rigid cylinders with elastic support. Exploring the FIV characteristics of a group of four flexible cylinders takes on vital importance in enhancing comprehension about the mutual interaction of multi-cylinder system. This paper mainly aims to perform a laboratorial study on FIV exhibited by four flexible cylinders positioned within a square geometric arrangement. Previous studies indicated that noteworthy mutual interference exists in the case of $P/D = 6.0$ (Huera-Huarte and Gharib, 2011; Xu et al., 2018a, 2018b). As a consequence, P/D was set as 6.0. Two representative scenarios involving incident angles of 0° and 45° were examined. A thorough exploration of the commonalities and distinctions within FIV characteristics of a group of four flexible cylinders and those of two or three flexible cylinders was undertaken and discussed by analysing the principal vibrations modes, response frequencies, displacement amplitudes, and motion trajectories.

The subsequent sections are structured as follows. Section 2 offers succinct overviews for the experimental arrangements. Section 3 outlines the methodology for data analysis. The outcomes for the two different incidence angle conditions are deliberated upon in Section 4. Ultimately, Section 5 provides concluding observations.

2. Experimental arrangements

Fig. 2 shows the experimental apparatus. The upper extremities of vertical supporting rods were affixed to the terminations of horizontal supporting structures. The lower ends of two vertical supporting rods were linked to the supporting plates, which provided necessary supports for the guide plates. The function of guide plates was to mitigate flow disturbances arising from the presence of vertical supporting rods and supporting plates. Within the support plate's central region and the guide plate's central region, apertures were integrated to accommodate installation of supporting plate dials and guide plate dials, respectively. One extremity of each model was equipped with a universal joint for installation, while the opposite end was linked to a steel wire across the pre-drilled cavity and routed through a pulley. The axial tension should be added at the end of flexible cylinder to resist the large IL deflections resulting from the mean drag. The value of pretension should not be too high because the large stiffness of flexible cylinder was not conducive to excite higher mode vibrations. As a compromise, the value of pretension was set as 450N.

Fig. 3 shows the sketch of a model consisting of an outer silicone tube and an internal copper pipe. The outer silicone, measuring 16 mm in diameter, snugly enveloped the internal copper pipe, ensuring smooth surface. The internal copper pipe, measuring 8 mm in diameter, was equipped with strain gages. A total of seven measuring positions were evenly distributed, with each of these points being equipped with four strain gages. Table 1 shows the primary parameters of cylinder models.

The experiment was performed within a tank that measured 137.0 m in length, 7.0 m in width, and had a depth of 3.3 m. The experimental apparatus was installed under a carriage that can move along the towing tank. The flexible cylinders were submerged in water and departs from the bottom and the free-surface at least 1.0m, which could avoid bottom effects and free-surface effects. The carriage traversed the length of the tank to create uniform flow conditions. Towing velocities spanned from 0.05 m/s to 1.00 m/s in increments of 0.05 m/s, corresponding to Reynolds numbers ranging from 800 to 16000. The velocity accuracy was 0.001 m/s. The velocity was set taking into account both the average deformation in IL direction and the vibration mode that can be excited. A high velocity is beneficial for exciting higher mode vibrations. However, the higher velocity would cause the larger average deformation of the model in IL direction, which could destroy the strain gages. The upper limit of flow velocity 1.0 m/s was determined by an iterative design. The flow velocity is high enough to excite the 3rd-order mode vibration in CF direction, and the IL average deformation dose not destroy the strain gages at the same time. Sampling was performed at 100 Hz, chosen to prevent the aliasing concerns. Data collection extended over a period of 50 s after achieving stable towing velocity. To ensure complete restoration of undisturbed water conditions, a 15-min interval was expended between consecutive runs. The initial spacing ratio remained constant at 6.0, and subsequently, the incidence angles were sequentially established at 0° and 45°. Alterations in the incidence angle were accomplished by rotating the dials shown in Fig. 2.

The structural nature frequencies were acquired from decay tests and shown in Table 2. It should be noted that the nature frequencies in two vibration directions were almost exactly the same and the IL nature frequencies were not presented here. As a comparison, Table 2 also includes the theoretical values calculated from Eq. (1).

$$f_n = \frac{n}{2L}\sqrt{\frac{T_c}{m_s + 0.25\rho\pi D^2} + \left(\frac{n\pi}{L}\right)^2 \frac{EI}{m_s + 0.25\rho\pi D^2}} \tag{1}$$

where n represents the mode number. It was found that the structural nature frequency of flexible cylinder model is dominated by the tension. The theoretical values demonstrated favorable correspondence with the measured values, falling well within the acceptable margin of error. The agreement demonstrates the dependability of both the experimental setup and the measuring system. The damping ratio was also obtained

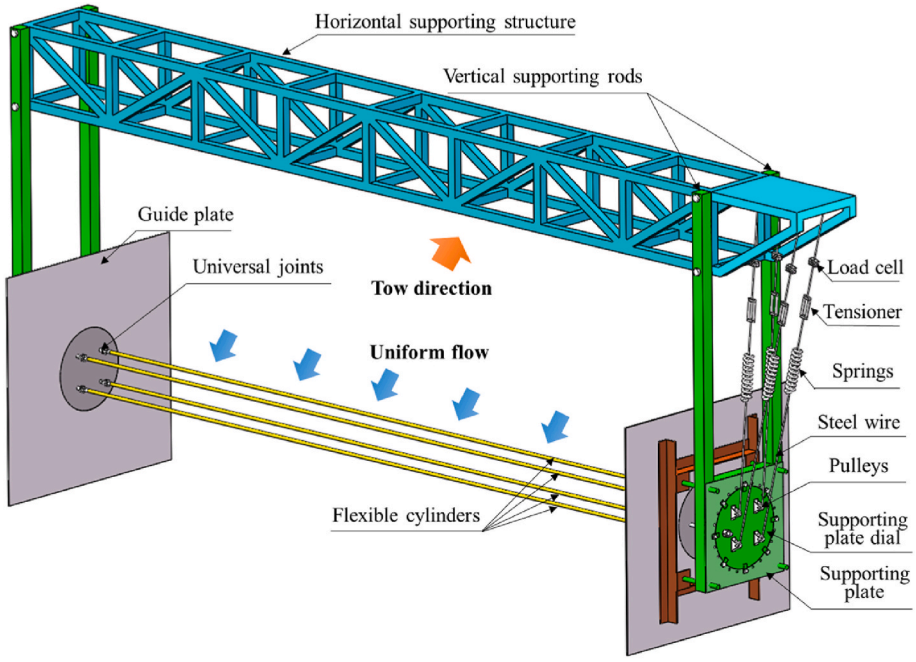

Fig. 2. Illustration of experimental apparatus.

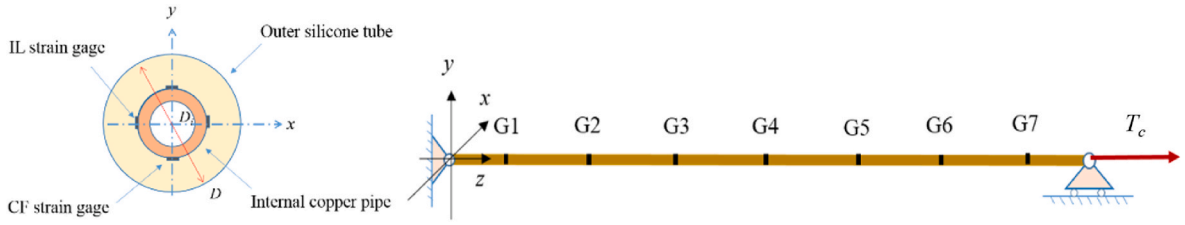

Fig. 3. An illustration of the arrangement of strain gages and the sketch of the cylinder model (Xu et al., 2018a).

Table 1
Primary parameters of the model (Ma et al., 2020; Xu et al., 2018a, 2018b).

Parameters	Values
Length, L	5.60 m
Diameter, D	0.016m
Aspect ratio, L/D	350
Mass per unit length, m_s	0.3821 kg/m
Mass ratio, m^*	1.90
Axial tension, T_c	450 N
Axial stiffness, EA	2.793×10^6 N
Bending stiffness, EI	17.45 Nm^2

Table 2
Structural nature frequencies in still water.

Mode number	Cylinder I	Cylinder II	Cylinder III	Cylinder IV	Theoretical values
f_1	2.49 Hz	2.54 Hz	2.56 Hz	2.64 Hz	2.49 Hz
f_2	4.78 Hz	4.70 Hz	4.83 Hz	4.75 Hz	5.08 Hz
f_3	7.81 Hz	7.41 Hz	7.58 Hz	7.42 Hz	7.84 Hz
f_4	10.51 Hz	10.42 Hz	10.61 Hz	10.55 Hz	10.85 Hz
f_5	14.21 Hz	13.80 Hz	14.11 Hz	13.98 Hz	14.16 Hz
f_6	17.66 Hz	17.60 Hz	18.09 Hz	17.88 Hz	17.85 Hz
f_7	22.91 Hz	22.01 Hz	22.35 Hz	22.28 Hz	21.95 Hz

from the decay tests. The damping ratio in water of the cylinder models is near 0.032.

3. .Data analysis

Modal analysis method, a commonly utilized displacement reconstruction technique, was applied to reconstruct the structural displacements. The strain data was pre-processed before using the modal analysis method. The half-bridge method was used to measure the strains, meaning that the temperature effect and the components due to the axial pretension could be ignored. The measured IL strains contain the mean components due to the mean drag, and the varying components due to IL VIV and the errors. The IL VIV strains vary with time, and the mean value in a period is close to zero. However, mean components due to the mean drag do not change with time and is basically close to a constant value at the same flow velocity. After eliminating the error by filtering, the IL VIV strains could be obtained by subtracting the mean value of filtered strain signals. The measured CF strains contain CF VIV strains and the errors. The CF strains could be obtained after filtering. A band-pass filter spanning the frequency range of 1.0–40.0 Hz was implemented to effectively eliminate inherent noise signals of both low and high frequencies.

The reconstruction process for CF displacement is presented for illustration. The CF displacement $y(z, t)$ can be formulated using Eq. (2) (Lie and Kaasen, 2006).

$$y(z,t)=\sum_{i=1}^{S}\chi_i(t)\Phi_i(z) \tag{2}$$

Where t represents time, $\chi_i(t)$ corresponds to modal weights, i signifies the modal order number, S denotes the highest order mode, $\Phi_i(z)$ stands for the mode shape. A sinusoidal function is employed for the simply supported boundary conditions.

$$\Phi_i(z)=\sin\frac{i\pi z}{L} \tag{3}$$

The displacements can be calculated according to the correlation between the strains and displacements.

$$\frac{\varepsilon(z,t)}{R}=\frac{\partial^2 y(z,t)}{\partial z^2}=\sum_{i=1}^{S}\chi_i(t)\frac{\mathrm{d}^2\Phi_i(z)}{\mathrm{d}z^2} \tag{4}$$

R represents the distance between strain gages from the structural neutral layer, and $\varepsilon(z, t)$ denotes strains. Rewrite Eq. (4) in a matrix form.

$$\Theta=\Omega\Upsilon \tag{5}$$

where

$$\Theta=\frac{1}{R}\left[\varepsilon(z_1,t)\quad \varepsilon(z_2,t)\quad \cdots\quad (z_M,t)\right] \tag{6}$$

$$\Omega=\begin{bmatrix}\Phi_1''(z_1) & \Phi_2''(z_1) & \cdots & \Phi_S''(z_1)\\ \Phi_1''(z_2) & \Phi_2''(z_2) & \cdots & \Phi_S''(z_2)\\ \vdots & \vdots & \ddots & \vdots\\ \Phi_2''(z_M) & \Phi_2''(z_M) & \cdots & \Phi_S''(z_M)\end{bmatrix} \tag{7}$$

$$\Upsilon=\left[\chi_1(t)\quad \chi_2(t)\quad \cdots\quad \chi_S(t)\right]^{\mathrm{T}} \tag{8}$$

where z_1, z_2, …, z_M denote the axial coordinate at the measuring positions, respectively. The modal weights can be calculated according to Eq. (9).

$$\Upsilon=\left(\Omega^{\mathrm{T}}\Omega\right)^{-1}\Omega^{\mathrm{T}}\Theta \tag{9}$$

After calculating modal weights, CF displacements were obtained by Eq. (2). The errors of the modal analysis method had been further analyzed in the previous research (Lie and Kaasen, 2006). It is found that the low order modes are very sensitive to the strain errors because the amplitudes of strain mode shapes are proportional to the mode number squared. The low order modes may introduce errors when the high order mode dominates the vibrations. The modes participating in the modal analysis should be selected cautiously to reduce the errors caused from the low order mode. Hence, some lower order modes were eliminated during the modal analysis, depending on the actual conditions.

4. Results and discussion

Principal vibration modes, vibration frequencies, displacement amplitudes and motion trajectories of four quadrilateral-arranged cylinders were examined for two distinct incidence angle scenarios in this section. Reduced velocities were calculated using the fundamental natural frequency f_1.

$$Ur=\frac{U}{f_1 D} \tag{10}$$

Considering the slight discrepancies among the measuring values, theoretical value of the fundamental natural frequency was employed in Eq. (10).

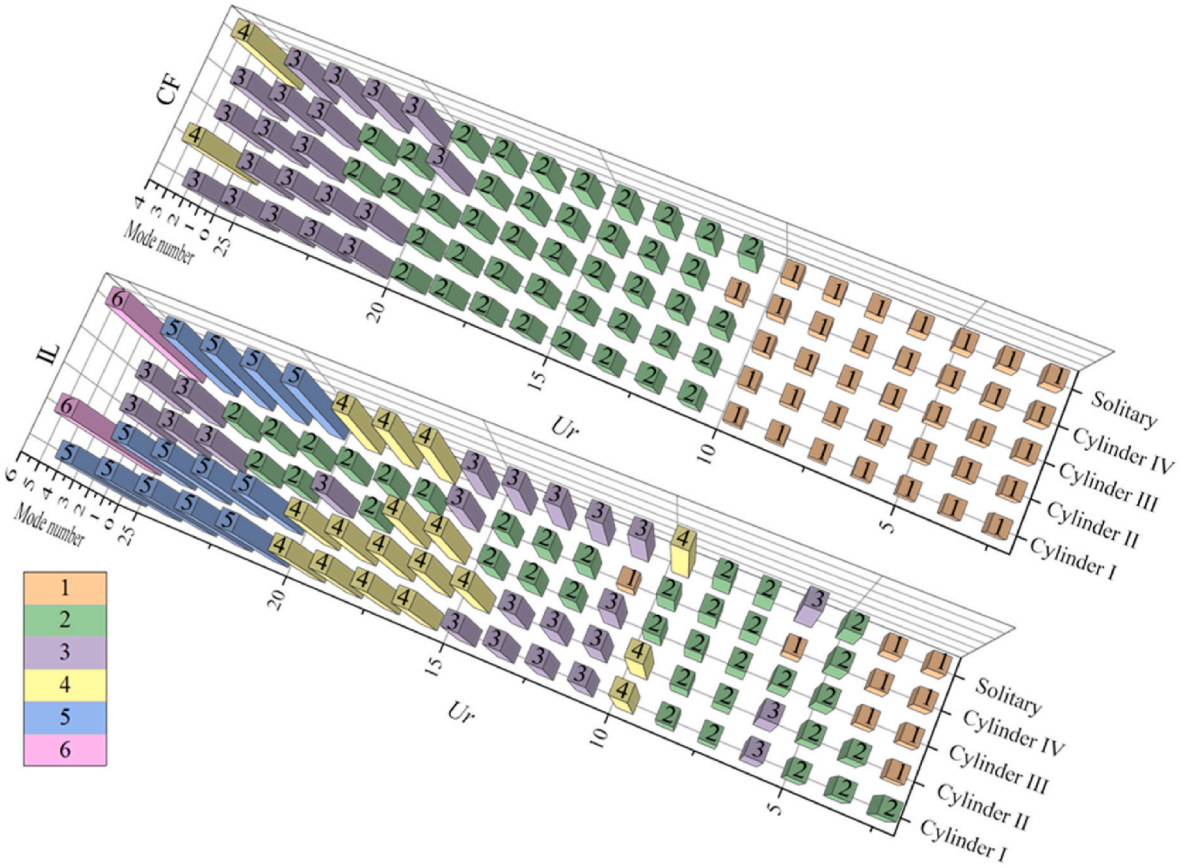

Fig. 4. The principal mode in two directions for $\beta = 0°$.

4.1. FIV responses for incidence angle 0°

As the *Ur* increased, multiple modes of vibrations were excited in the four flexible cylinders due to their possessing multiple-order natural frequencies. Fig. 4 displays the principal mode in CF and IL vibrations at $\beta = 0°$. Principal modes were identified as the modes with the highest modal weight. The principal modes of the solitary flexible cylinder undergoing VIV were also included as a comparison. In Fig. 4, distinct colours are used to distinguish different principal modes, progressing from lower to higher orders. During the VIV of a solitary cylinder, the first four mode are triggered in CF direction. The principal modes in CF vibrations of the upstream cylinders I and II exhibit similarities to those of the solitary cylinder. When the flexible cylinders are positioned side-by-side, Xu et al. (2018a) has been verified that the higher-order mode is prone to being excited more readily in mode switching region, contrary to findings regarding the upstream cylinders I and II. The discrepancy implies that the downstream cylinders could impede the premature excitation of higher-order modes for the upstream cylinders I and II. The activation of the higher-order mode in downstream cylinders III and IV is postponed because of the wake shielding effect generated from cylinders I and II, which aligns with conclusions drawn from observations made in the downstream cylinder of a tandem cylinder system (Xu et al., 2018b). As an instance, oscillations of cylinders III and IV are primarily governed by the 2nd-order mode at $Ur = 20.04$ and 21.29. Meanwhile, the 3rd-order mode is principal in oscillations of the upstream cylinders I and II.

Compared to oscillations in CF direction, oscillations in IL direction typically stimulate modes of higher orders. The high-order mode vibrations usually involve serious mode competitions (Chaplin et al., 2005), leading to mode jumps in the oscillations of the solitary cylinder at $Ur = 5.01$ and 8.77. The IL principal modes of cylinders I and II exhibit notable resemblances to those of the solitary cylinder, except for some slight differences observed in the initial region and mode switching region. However, the IL principal modes of cylinders III and IV are significantly affected by the upstream cylinders I and II. When *Ur* is below 7.52, the principal modes in IL oscillations of the downstream cylinders III and IV display only minor deviations compared to the solitary cylinder. As the *Ur* increases, distinctions in principal modes between downstream cylinders and a solitary cylinder become evident. In the case of $Ur = 11.27$–25.05, the IL vibrations of the cylinders III and IV exhibit lower principal modes when contrasted with cylinders I and II. Specifically, the principal mode in IL oscillations of the cylinders III and IV often corresponds to the second order at various *Ur* values, while the highest observed principal mode reaches up to the 4th-order.

Fig. 5 illustrates the dimensionless principal frequencies in the case of $\beta = 0°$. Notably, the principal frequencies in CF oscillations for all the cylinders I, II and the solitary cylinder exhibit an increase as *Ur* rises. The occurrence of a mode switch is associated with a noticeable increase in principal frequencies. The CF principal frequencies of cylinders I and II exhibit a remarkable similarity to those of the solitary cylinder, which agrees well with the outcomes observed in studies involving a two cylinder system positioned side-by-side. When *Ur* is lower than 15.03, principal frequency in CF direction of the downstream cylinders III and IV conforms to a comparable variation pattern as observed in the solitary cylinder. As *Ur* increases, the downstream cylinders III and IV have lower CF principal frequencies in contrast to those of the upstream cylinders, aligning with the conclusions drawn from the principal mode shown as Fig. 4. The phenomenon characterized by decreased principal frequencies of downstream cylinder was also noted in studies involving two tandem cylinders. It is verified that the reduction of principal frequency mainly resulted from the wake shielding effects (Xu et al., 2018b; Ma et al., 2019; Xu et al., 2018).

The IL principal frequencies roughly increase with *Ur*, except for the cases where mode jump occurs. The principal frequencies in IL oscillations of upstream cylinders I and II demonstrate a strong concordance with those observed in the solitary cylinder. Conversely, the IL principal

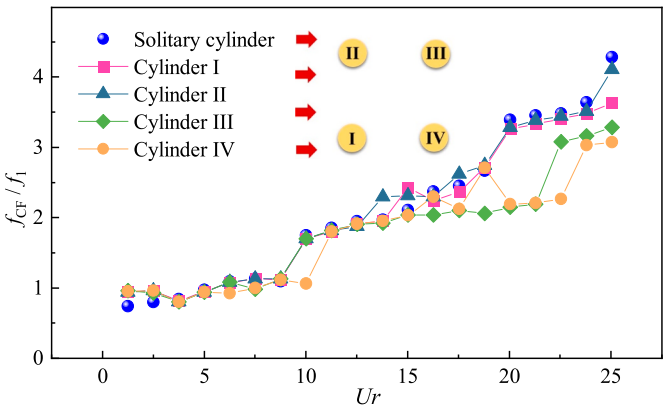

(a) CF dimensionless principal frequencies versus *Ur*.

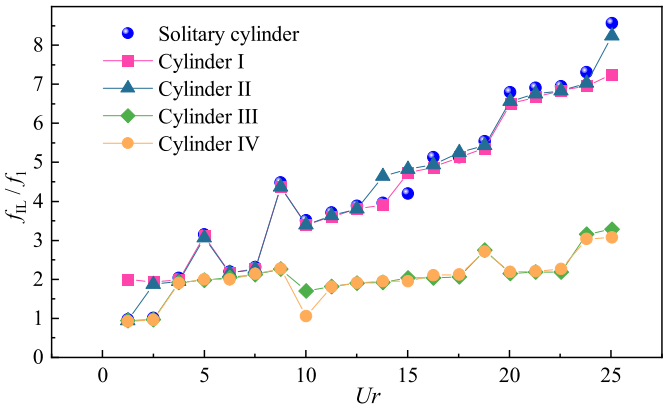

(b) IL dimensionless principal frequencies versus *Ur*.

Fig. 5. Dimensionless principal frequencies of the four flexible cylinders when the incidence angle $\beta = 0°$.

frequencies of downstream cylinders III and IV undergo a significant reduction. However, IL principal frequency of downstream cylinder just slightly decreased when two flexible cylinders were positioned in a tandem configuration (Xu et al., 2018b). This observation contrasts with the outcomes derived in the IL oscillations of cylinders III and IV, indicating that the obvious decrease in IL principal frequencies is not solely attributed to the wake shielding effect. Within a quadrilateral-arranged cylinder system, oscillations of the downstream cylinders are subject to a combined influence originating from two upstream cylinders. Under the combined wake interference, the IL principal frequencies cease to maintain a twofold relationship with the CF principal frequencies. For downstream cylinders III and IV, a new proportional relation with a value near 1.0 is established between the principal frequencies in the two directions.

The vibration frequencies at measuring positions of cylinders II and III in the case of $\beta = 0°$ are presented to further discuss the frequency characteristics, shown in Fig. 6. The subplots presented in Fig. 6 are organized in rows, with each row corresponding to a distinct measuring position. G1 ~G7 are arranged from the uppermost row to the lowest. The vibration frequency is plotted along the horizontal axis, while the power spectral density (PSD) is represented on the vertical axis. To concentrate on the vibrations associated with high-order modes, a reduced velocity of 21.29 has been chosen. For cylinder II, the CF principal mode is the 3rd-order with a principal frequency of 8.42 Hz at $Ur = 21.29$. While, IL principal mode is the 5th-order with a principal frequency of 16.83 Hz, nearly twice the magnitude of the CF principal frequency. An incidental and weak harmonic component with a

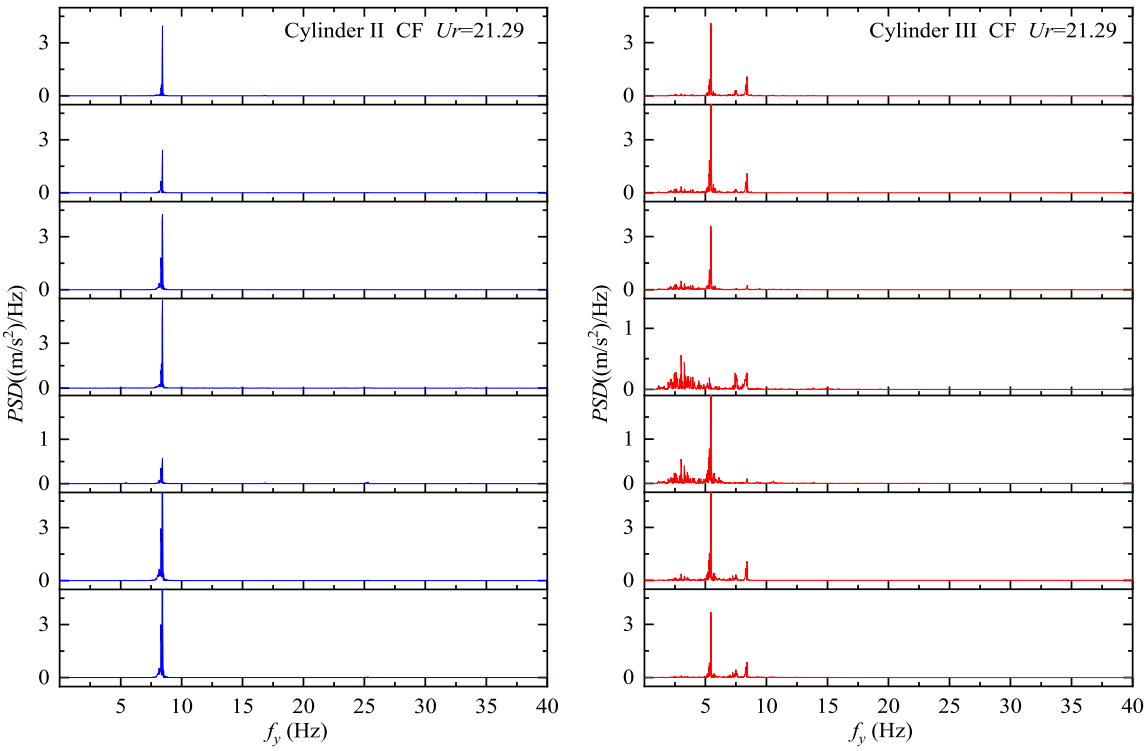

(a) CF vibration frequency of cylinder II at *Ur*=21.29. (b) CF vibration frequency of cylinder III at *Ur*=21.29.

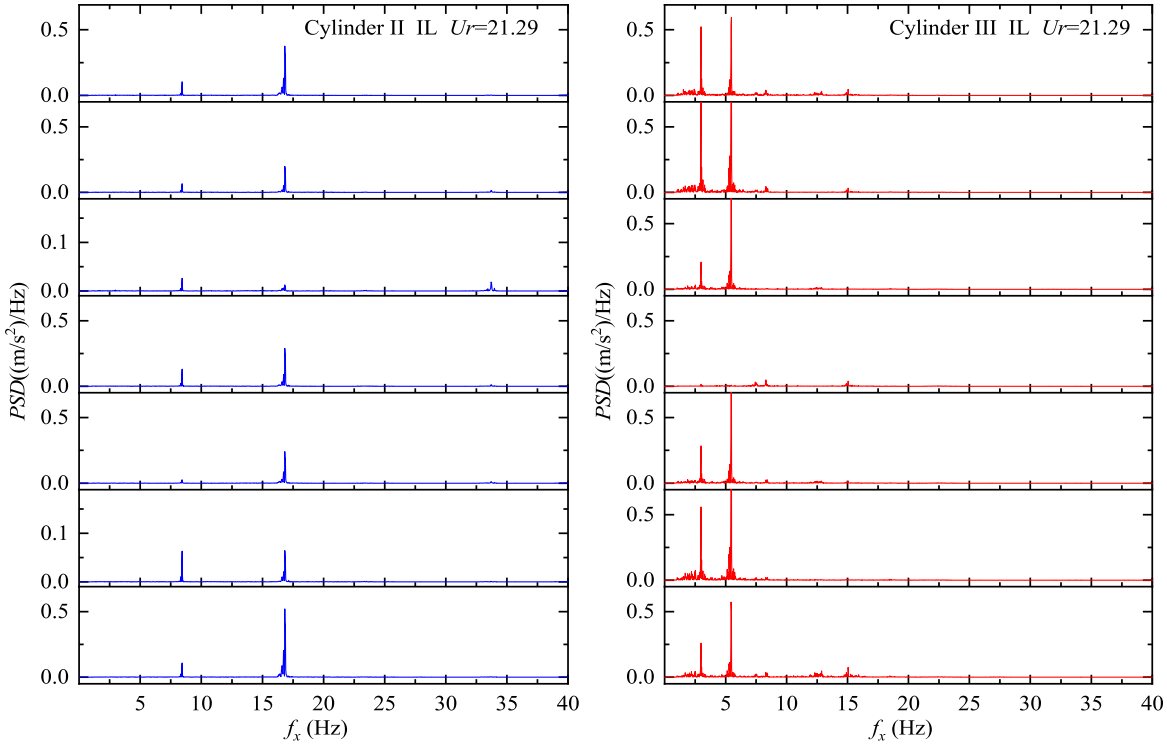

(c) IL vibration frequency of cylinder II at *Ur*=21.29. (d) IL vibration frequency of cylinder III at *Ur*=21.29.

Fig. 6. CF and IL vibration frequencies at measuring positions of the four flexible cylinders for incidence angle 0°.

frequency of 8.42 Hz is also discernible within the IL vibrations of cylinder II. It can be certified that the frequency feature of upstream cylinders bear resemblance to that observed in the solitary flexible cylinder.

The CF principal frequency of cylinder III is 5.45 Hz, which shows a distinct reduction from that of cylinder II under an equivalent reduced velocity condition. A weak frequency component of 8.42Hz, corresponding to the CF principal frequency of cylinder II, emerges owing to wake interactions from the leading cylinder. The phenomenon has been documented in the studies involving the oscillations in a pair of tandem cylinders (Xu et al., 2018b). Oscillation in IL direction of cylinder III has two notable frequency components. The first one has a value of 2.98 Hz, while the second one matches the CF principal frequency of 5.45 Hz. The IL frequency characteristic displayed by the downstream cylinder within a four flexible cylinder system at $\beta = 0^\circ$ has not been encountered in the investigation concerning two tandem flexible cylinders. Further discussed will be undertaken by considering the outcomes of the response amplitude and motion trajectory.

Fig. 7 depicts the max root mean square (RMS) of displacements for four flexible cylinders at $\beta = 0^\circ$. The RMS values of vibration amplitudes at a specific spanwise location, denoted as z_i, are calculated over time.

$$y_{rms}(z_i) = \sqrt{\frac{1}{K}\sum_{j=1}^{K} y(z_i, t_j)^2} \tag{11}$$

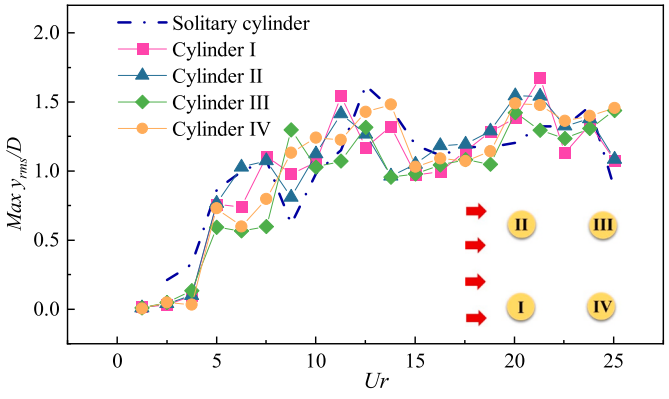

(a) Max RMS of dimensionless displacements in CF direction.

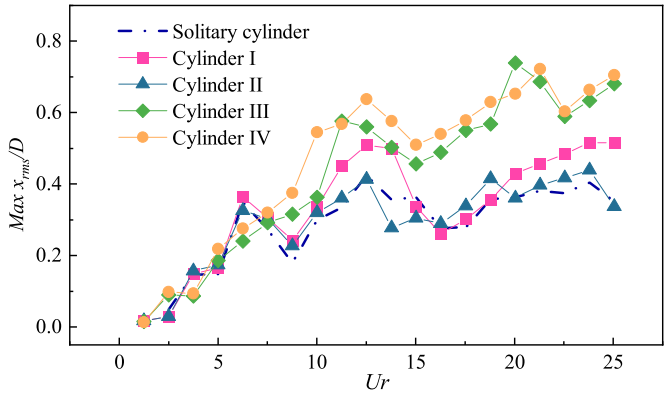

(b) Max RMS of dimensionless displacements in IL direction.

Fig. 7. Max RMS of displacements for four flexible cylinders when the incidence angle $\beta = 0^\circ$.

$$x_{rms}(z_i) = \sqrt{\frac{1}{K}\sum_{j=1}^{K} \left[x(z_i, t_j) - x_{mean}\right]^2} \tag{12}$$

where K is the sampling number, x_{mean} is the mean displacement resulting from the mean drag. The max RMS value of dimensionless displacements in two directions is employed to portray the intensities of FIV response.

The outcomes from a solitary flexible cylinder are presented for comparison. As illustrated in Fig. 4, oscillations in CF direction of a solitary cylinder successively excite the initial four order modes. The maximum y_{rms}/D of a solitary cylinder initially rises to its pinnacle and subsequently decreases consistently within the mode-synchronized regions, aligning with findings from previous investigations (Song et al., 2011; Trim et al., 2005). The maximum y_{rms}/D values of cylinders I and II closely resemble those of a solitary cylinder until reaching a peak value within the 1st-order mode-synchronized region. As *Ur* increases, the maximum y_{rms}/D of cylinders I and II gradually departs from findings observed in a solitary cylinder, owing to the influence of the proximity effect (Zdravkovich, 1985). However, variations in maximum y_{rms}/D of cylinders I and II still follow an identical trend except for some certain values. It has been demonstrated that the proximity effect could result in the asymmetric wake when two flexible cylinders are arranged side-by-side (Han et al., 2018b), which gives rise to the discrepancy between cylinders I and II. Cylinder III follows a comparable pattern in the maximum y_{rms}/D as observed in cylinder IV. The maximum y_{rms}/D of cylinder IV exhibits a slight increment compared to that of cylinder III, indicative of the influence of the proximity effect. Further validation of the proximity effects is established through a comparative analysis between the outcomes of the downstream cylinders III and IV within the a four-cylinder system and the results derived from the downstream cylinder within a pair of tandem cylinders. The maximum y_{rms}/D values for cylinders III and IV closely resemble those of the downstream cylinder a pair of tandem cylinders when *Ur* is below 15.03. The influence of the proximity effect intensifies as *Ur* increases, resulting in significantly larger maximum y_{rms}/D values for cylinders III and IV in comparison to both a solitary cylinder and a downstream cylinder within a pair of tandem cylinders (Xu et al., 2018b). Under wake interference, variations in maximum y_{rms}/D for cylinders III and IV diverge from those exhibited by the solitary cylinder. Specifically, within the mode-synchronized region of the 1st-order mode, cylinders III and IV display lower displacements compared to the solitary cylinder. The maximum y_{rms}/D values for cylinders III and IV experience an increment following the attainment of a peak in the outcomes of a solitary cylinder. Similar variations in CF dimensionless displacement have also been noted in a study concerning FIV of four quadrilateral-arranged rigid cylinders with elastic support (Gao et al., 2019). The oscillations for the downstream rigid cylinders with elastic support undergo a substantial augmentation as *Ur* rises, resembling the FIV response observed in downstream cylinder within two tandem rigid cylinders with elastic support. However, the continued substantial growth in the CF displacements is not is not apparent in the downstream flexible cylinders. This trend is consistent with findings from earlier investigations on FIV of a pair of tandem flexible cylinders (Huera-Huarte et al., 2016; Xu et al., 2018b), where it was confirmed that oscillation amplitudes in CF direction of the downstream cylinder do not experience significant enlargement owing to the excitation of higher-order mode vibrations.

Cylinders I and II exhibit a similar pattern in the maximum x_{rms}/D values, aligning with the trend observed for a solitary cylinder, as shown in Fig. 7(b). The maximum x_{rms}/D values for cylinders I and II closely match those of the solitary cylinder when *Ur* is below 10.02. As *Ur* increases, both cylinders I and II show heightened vibration displacements in contrast to the solitary cylinder, owing to the influence of the proximity effect. It has been pointed that there remains a significant interaction in IL direction between a pair of flexible cylinders positioned side-

by-side with P/D below 8.0, which would amplify IL displacements (Xu et al., 2018a). The maximum x_{rms}/D values for cylinders III and IV exhibit substantial increments in comparison to a solitary cylinder, which is of great concern. Different from the solitary cylinder, cylinders III and IV have continued increase in the maximum x_{rms}/D until the maximum x_{rms}/D reaches its first peak at $Ur = 11.27$ and 12.52 respectively. The vibrations corresponding to the 2nd-order mode become stimulated as Ur increases further, and the maximum x_{rms}/D of cylinders III and IV remain growth until the maximum x_{rms}/D reaches its second peak at $Ur = 20.04$ and 21.29 respectively. Although oscillations in IL direction of cylinders III and IV are characterized by lower modes and frequencies, as illustrated in Figs. 4 and 5, the extreme values of x_{rms}/D for cylinders III and IV are notably amplified by 76% and 71%, respectively, in comparison to the solitary cylinder. The notable augmentation in IL oscillations absents for a downstream flexible cylinder within a pair of tandem cylinders (Huera-Huarte et al., 2016; Xu et al., 2018b). This discrepancy suggests that the configuration of four quadrilateral-arranged flexible cylinders cannot be equated to two sets of tandem cylinders arranged in parallel. The two upstream cylinders collectively exert substantial impacts on the oscillations in IL direction of downstream cylinders. Notably elevated displacements in IL direction are also apparent for downstream cylinders within four quadrilateral-arranged rigid cylinders, the increasing IL displacements are attributed to the intricate interplays arising from the shear layers detached from a pair of upstream cylinders and the mutual vortex shedding from a group of four cylinders (Gao et al., 2019).

Fig. 8 displays the contour plot of dimensionless displacements, axial distribution plots of the RMS values, and temporal history curves at measuring positions of the four flexible cylinders for incidence angle 0°. In order to examine the behaviours of high-order mode vibrations, a reduced velocity of 21.29 is selected. It becomes evident that the oscillation response for the pair of upstream cylinders I and II exhibit a remarkable similarity. The contour plots of dimensionless displacements indicate that vibrations in both two directions of cylinders I and II encompass the hybrid feature of both standing and traveling wave. The axial distribution plot of CF RMS displacements displays asymmetry, a characteristic caused by the presence of multi-mode vibrations (Song et al., 2011). The 3rd-order mode predominantly governs CF vibration, while the 5th-order mode dominates IL vibration. Both the CF and IL vibrations have a better periodicity though some harmonic components are observed. Noteworthy harmonic responses are evident in CF vibrations, particularly at measuring positions situated in proximity to the nodes in the axial distribution plot of the RMS displacements. The harmonic responses are more prominent in IL direction, which is in accordance with the spectral findings presented in Fig. 6(c). It is observed that the downstream cylinders III and IV have different features in the FIV responses. The variations in the contour plots of dimensionless displacements are slightly more disordered than those of the upstream

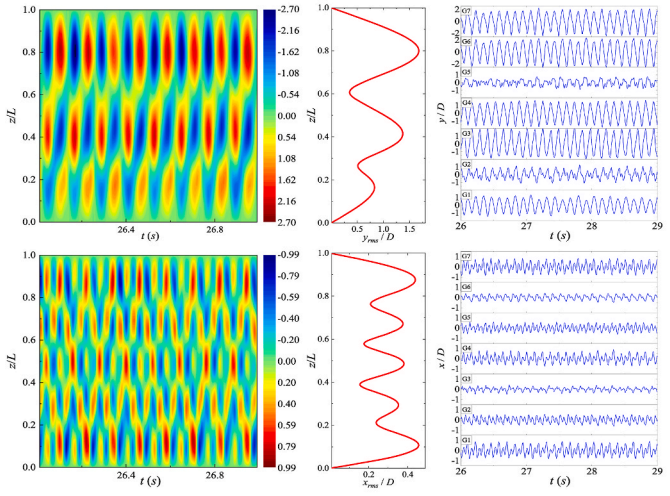

(a) Cylinder I at Ur=21.29.

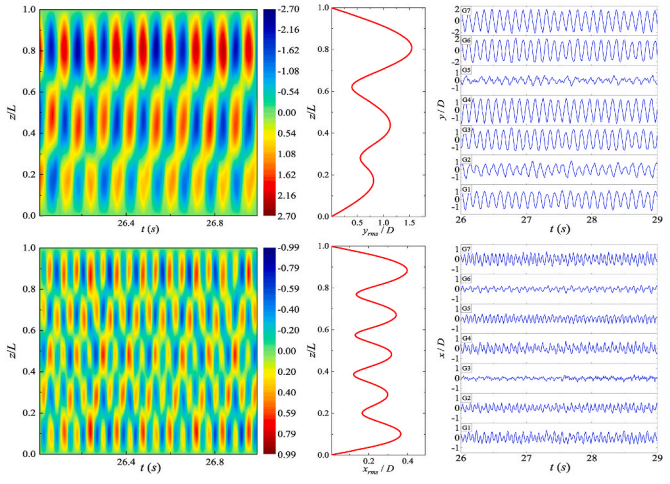

(b) Cylinder II at Ur=21.29.

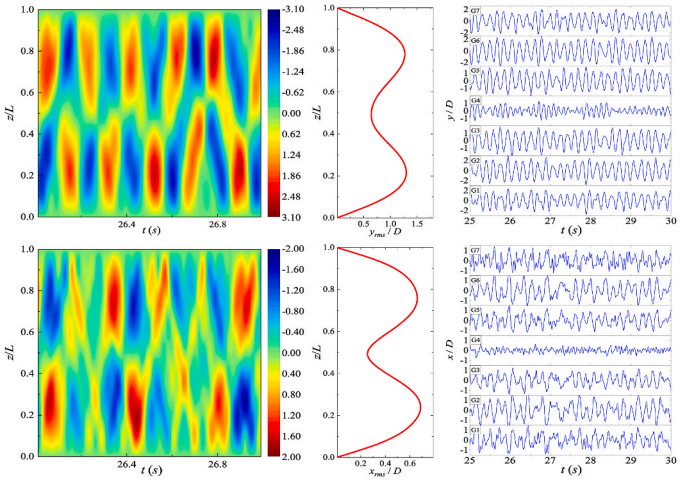

(c) Cylinder III at Ur=21.29.

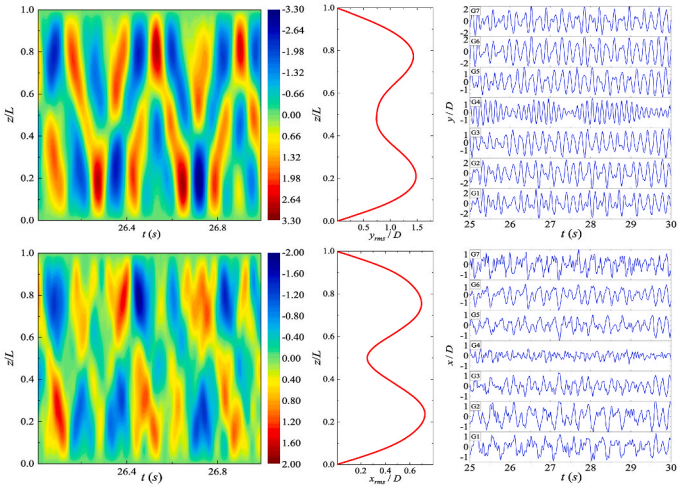

(d) Cylinder IV at Ur=21.29.

Fig. 8. Contour plot of dimensionless displacements, axial distribution plot of the RMS displacements, and temporal history curves of displacement at measuring positions of the four flexible cylinders for incidence angle 0°.

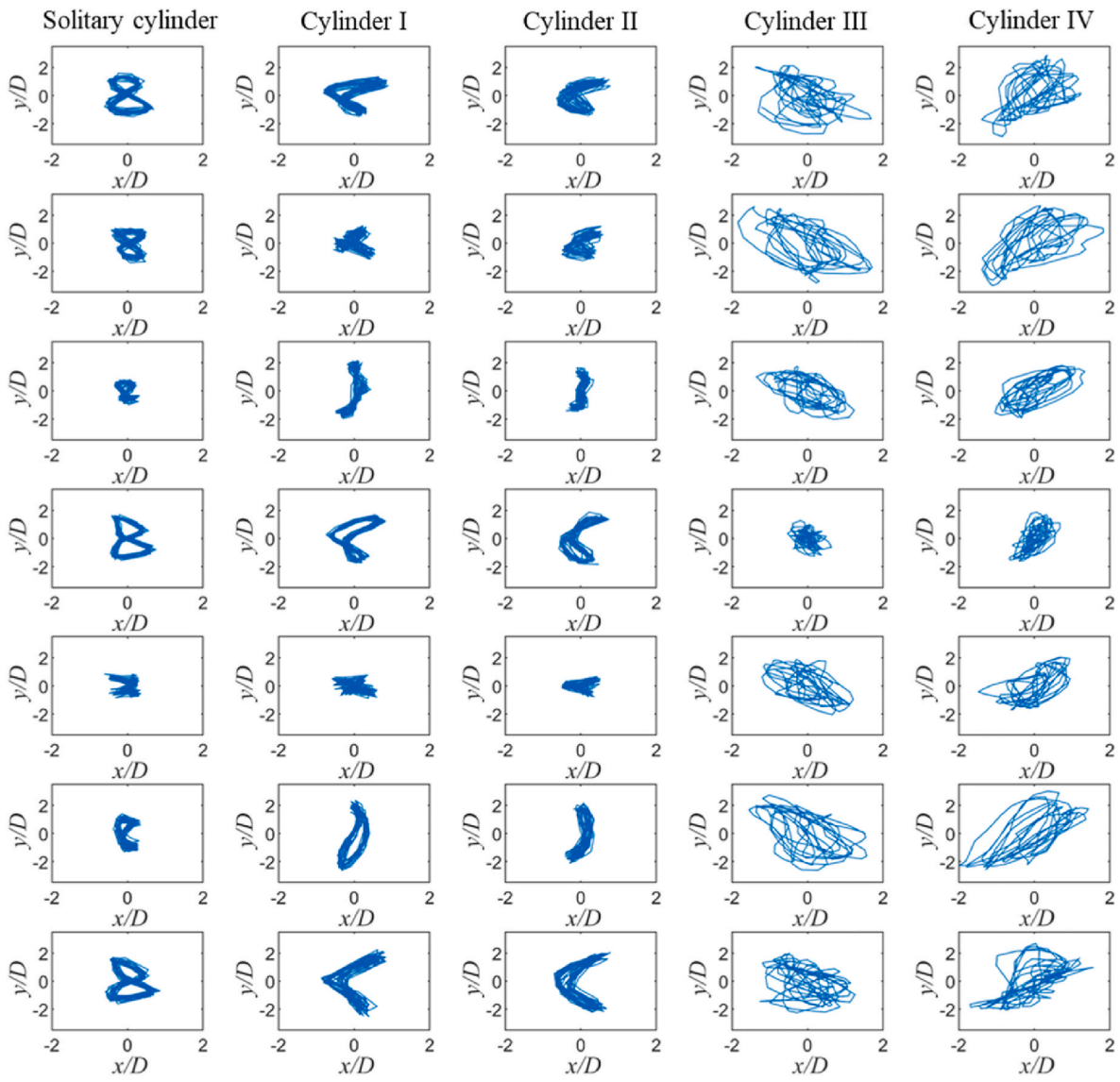

Fig. 9. Motion trajectories of four cylinders at measuring positions in the case of $\beta = 0°$.

cylinders. Hybrid features of standing and traveling wave are discernible for both CF and IL directions. Analysing axial distribution plot of RMS displacements, it becomes evident that the principal vibration mode of downstream cylinders III and IV is of lower order than that observed in upstream cylinders I and II. The oscillations in two directions have an identical principal mode of 2nd-order, a departure from the findings involving the solitary cylinder and a pair of flexible cylinders. The periodicity of the CF and IL vibrations becomes significantly weak due to the multiple harmonic components.

Fig. 9 shows motion trajectories of four cylinders at measuring positions in the case of $\beta = 0°$, and G1 ~G7 are arranged from the uppermost row to the lowest. The time history range of the motion trajectory is during 26s–29s. The motion trajectories of the solitary cylinder form a pattern resembling the figure-eight shape, suggesting that the frequencies in IL oscillations are roughly double those in CF oscillations. The upstream cylinders I and II exhibit analogous motion trajectories characterized by figure-eight shape and C shape. Compared to the solitary flexible cylinders, the motion trajectories of the two upstream cylinders are disturbed due to the proximate effect. For example, motion trajectories of a solitary cylinder at the following measuring positions G1, G2, G3, G4 and G7 exhibit the typical pattern of figure-eight shape. While, the upstream cylinders at the above measuring positions display motion trajectories with notable distortions. In contrast to either a solitary cylinder or an upstream cylinder, downstream cylinders III and IV exhibit much more disordered motion trajectories. Most of the motion trajectories are an elliptical shape, although their repeatability is compromised due to the presence of oscillations characterized by multiple frequencies and amplitudes.

The motion trajectories of the elliptical shape are attributed to the close resemblance between the principal frequency in two directions. For the four quadrilateral-arranged rigid cylinders with elastic support (Gao et al., 2019), elliptical shape motion trajectories with large IL displacements are also observed for the two downstream cylinders within the unique resonance region. The present investigation provides further confirmation that the vibrations of the downstream flexible cylinders continue to exhibit substantial amplitudes and low frequencies in IL direction and motion trajectories of an elliptical shape. The phenomenon has been elucidated by analysing wake flow patterns using a numerical approach (Gao et al., 2019). For four quadrilateral-arranged cylinders in the case of $\beta = 0°$, the vortices released by the pair of upstream cylinders are in synchronization with each other. The interconnected wake patterns originating from upstream cylinder would persistently collide with the downstream cylinder and amalgamate into the vortices released from two downstream cylinders, resulting in the

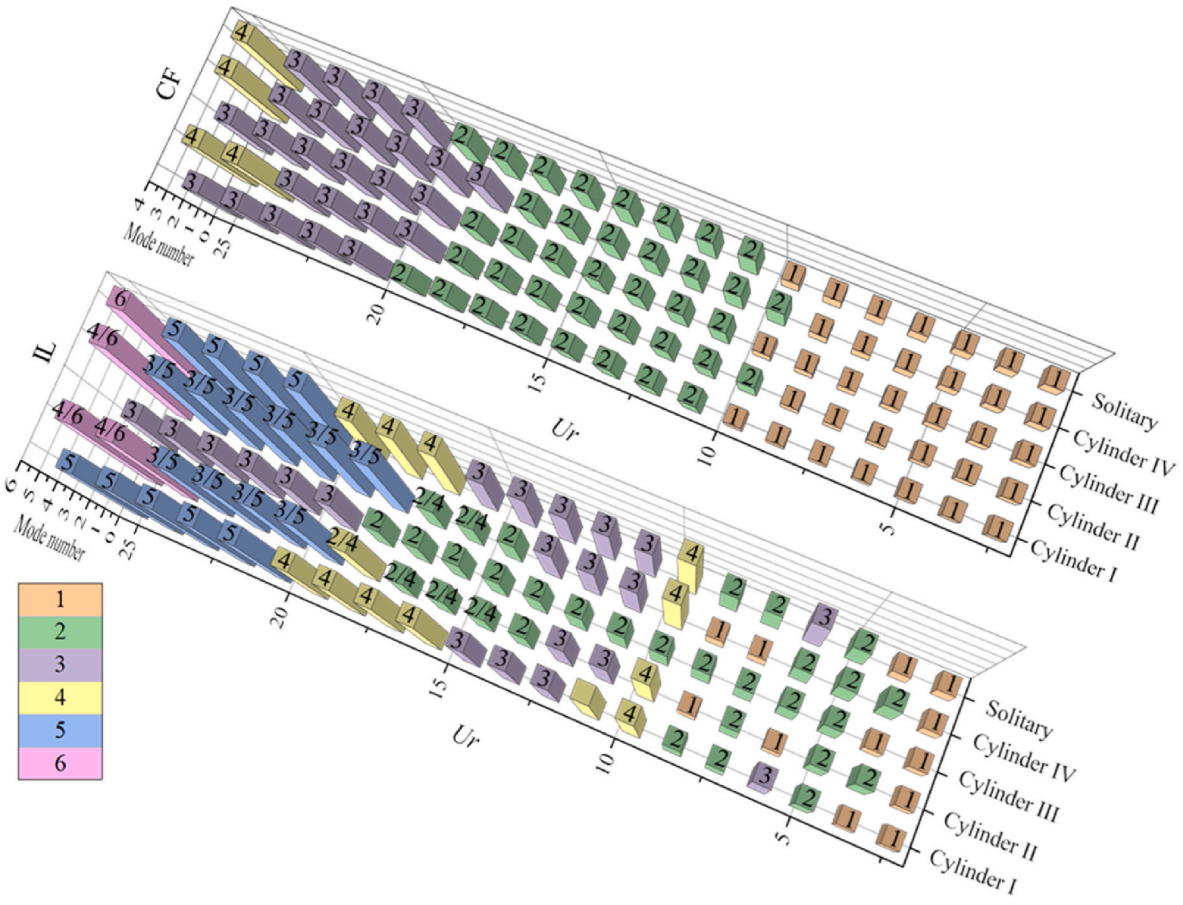

Fig. 10. The principal mode in two directions for $\beta = 45°$.

different FIV response characteristics.

4.2. FIV responses for incidence angle 45°

The incidence angle 45° is considered one of the common incidence angles in the arrangement of four quadrilaterally positioned flexible cylinders. Fig. 10 displays the principal mode in CF and IL vibrations when the incidence angle $\beta = 45°$. It appears that there are minor discrepancies in the principal modes of CF oscillations between the solitary cylinder and the four flexible cylinders. Cylinder I is positioned as the upstream cylinder within the grouping of four flexible cylinders, and its principal modes in CF direction closely resemble those of the upstream cylinder within the three flexible cylinder system positioned in a triangular arrangement (Ma et al., 2019). Cylinders II and IV are side-by-side arranged between cylinders I and III. The excitation of higher-order mode oscillations in CF direction occurs earlier for cylinders II and IV, primarily attributed to the influence of wake interference and proximity effects. For example, cylinder IV exhibits the 2nd- and 3rd-order mode oscillations in CF direction at $Ur = 8.77$ and 17.57, respectively. While the solitary cylinder exhibits the 2nd- and 3rd-order mode oscillations in CF direction at slightly higher velocities $Ur = 10.02$ and 20.04, respectively. Cylinder III, positioned as the downstream cylinder within the grouping of four quadrilaterally positioned flexible cylinders, experiences influence from the upstream cylinders that is not captured solely through the analysis of principal mode in CF oscillations.

The IL principal modes of cylinder I exhibit strong similarity to those of the solitary cylinder except at $Ur = 10.02$, 16.28 and 25.05, suggesting that the existence of downstream cylinders minimally affects behaviours of the upstream cylinder. When Ur exceeds 13.78, significant disparities become evident in the IL principal modes of cylinders II and IV compared to those of the solitary cylinder. Some square columns in Fig. 10 are annotated with numerical labels, indicating that the vibrations are primarily governed by two distinct modes possessing nearly equivalent modal contributions. For example, the notation 2/4 signifies joint dominance of the 2nd- and 4th-order modes in IL direction. As Ur rises, the IL vibrations of cylinders II and IV exhibit multiple principal modes, such as the combination of 2/4, 3/5 and 4/6.

To provide the better understanding of modal contributions, Fig. 11 shows RMS of modal weights in IL vibrations of both the solitary cylinder and cylinder IV at $Ur = 21.29$ and 25.05. It is observed that the modal weights corresponding to the 5th- and 6th-order modes distinctly surpass those of modes with other orders at $U_r = 21.29$ and 25.05 respectively, indicating a single vibration mode unequivocally takes precedence and dominates the overall vibration behaviours of the solitary cylinder at a certain Ur. Though the 5th- and 6th-order modal weights have the highest value of RMS at $U_r = 21.29$ and 25.05 respectively, it is important to note that the oscillations of cylinder IV do not exhibit exclusive dominance by a single vibration mode. At $U_r = 21.29$, the value for the 3rd- and 5th-order modal weights is 0.33 and 0.36, respectively. Both the 3rd- and 5th-order mode assert their dominance, as they are both prominent in this scenario, resulting in a shared control over the vibration behaviours. The similar result that multiple vibration modes dominate the IL vibrations together is also observed for cylinder IV at $U_r = 25.05$.

Fig. 12 shows the time-frequency graph of the IL displacement of cylinder IV. The vertical axis denotes the frequency, and the horizontal axis denotes the time. The color bar represents the wavelet coefficient, which is positively correlated with the energy of the frequency component. Two velocity cases were selected as examples, namely $Ur = 21.29$ and 25.05. In each velocity case, the measuring position G3 was

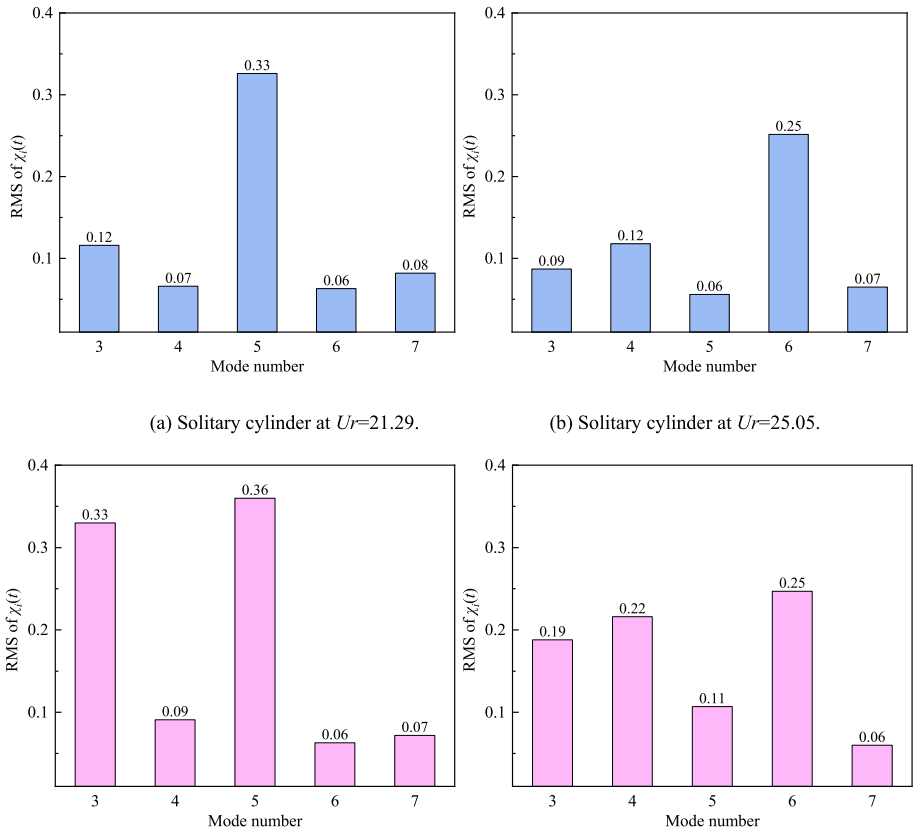

(a) Solitary cylinder at *Ur*=21.29. (b) Solitary cylinder at *Ur*=25.05.

(c) Cylinder IV at *Ur*=21 29 (d) Cylinder IV at *Ur*=25 05

Fig. 11. RMS of IL modal weights for a solitary cylinder and cylinder IV.

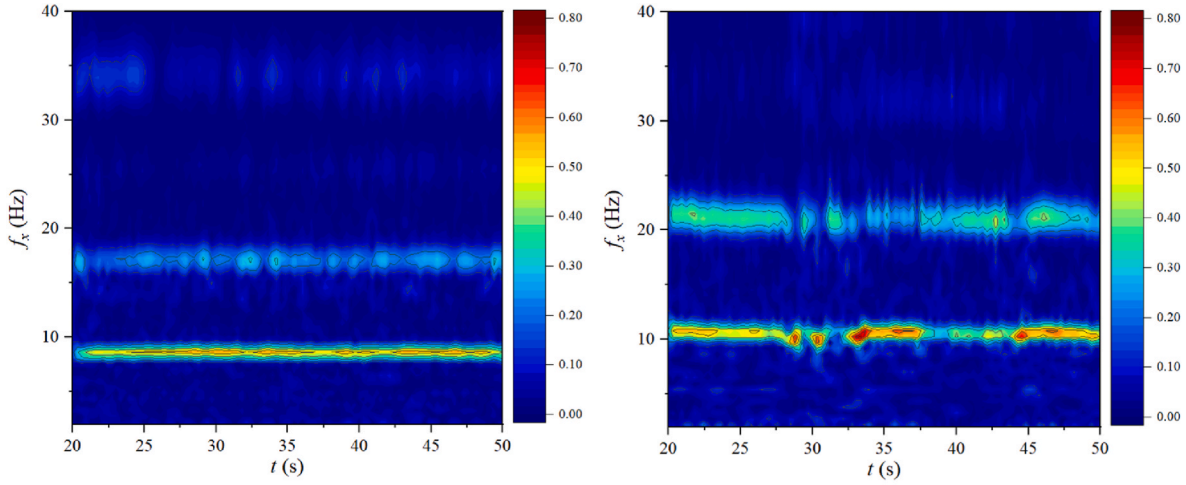

(a) *Ur*=21.29. (b) *Ur*=25.05.

Fig. 12. Time-frequency graph of the IL displacement of cylinder IV.

selected. At Ur = 21.29, cylinder IV displays two distinct frequency components that are relative to the 3rd- and 5th-order vibration modes, respectively. The two frequency components persist for the entire time period of the test. The frequency component of 17.0Hz shows a clear intensity change with time, while intensity change of the frequency component with 8.60Hz requires careful observation to detect. At Ur = 25.05, the two frequency components are relative to the 4th- and 6th-order mode vibration modes, respectively. The intensity peaks of the two frequency components show remarkable alternate changes, indicating the presence of the mode competition.

The phenomenon of multiple vibration principal modes has also been found in two adjacent downstream cylinders within a flexible cylinders system arranged in a triangular configuration (Ma et al., 2019). It has been verified that the presence of multiple principal mode responses in IL direction primarily arises from wake interference created from an upstream cylinder, as opposed to the proximate effect originating from a

nearby neighbouring cylinders (Ma et al., 2019; Xu et al., 2018a). Cylinder III's IL principal modes exhibit dissimilarities in comparison to both the remaining three cylinders and the solitary cylinder. The stable evolution of the IL principal mode with respect to *Ur* is attributed to influences of the three upstream cylinders, precluding occurrence of mode jumps. As *Ur* exceeds 11.27, the principal modes in IL direction of cylinder III exhibit notably lower magnitudes compared to those of a solitary cylinder. A previous observation indicates that the downstream cylinder positioned behind two upstream adjacent cylinders appears multiple principal mode responses in IL direction (Ma et al., 2019), inconsistent with the outcomes of cylinder III. This disparity arises from the fact that wake interference between cylinders II and IV is disrupted by the upstream cylinder I, subsequently leading to the modifications for vibration responses in downstream cylinder III.

Fig. 13 displays the dimensionless principal frequencies in the case of $\beta = 45°$. The principal frequencies in CF direction of cylinder I exhibit a remarkable similarity to those of the solitary cylinder, in accordance with findings regarding the principal modes of cylinder I. Cylinders II and IV are positioned adjacently in a side-by-side configuration. Minor distinctions are observed in the CF principal frequencies between cylinders II and IV owing to their close proximity. Notably, when the principal vibration mode transitions, cylinders II and IV exhibit slightly higher CF principal frequencies compared to the solitary cylinder. This phenomenon can be ascribed to the occurrence of higher-order mode vibrations being initiated earlier for cylinders II and IV. The CF principal frequencies of cylinder III are mildly affected by the remaining upstream cylinders when *Ur* is below 15.03. With the increase of *Ur*, principal frequencies in CF direction of cylinder III progressively diverge from the

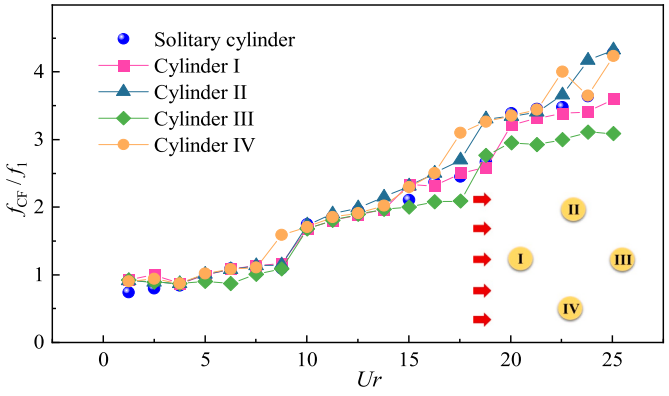

(a) CF dimensionless principal frequencies versus *Ur*.

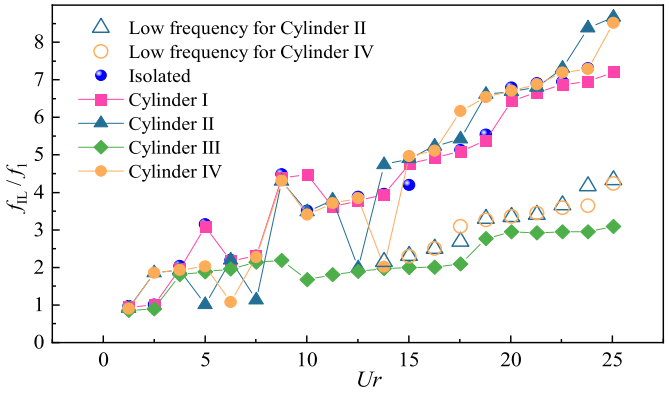

(b) IL dimensionless principal frequencies versus *Ur*.

Fig. 13. Dimensionless principal frequencies of the four flexible cylinders when the incidence angle $\beta = 45°$.

outcomes observed in the solitary cylinder, ascribing the wake interference generated by the remaining three cylinders. Although the CF principal modes remain consistent between cylinder III and the solitary cylinder, the principal frequencies in CF direction of cylinder III significantly decrease compared to the solitary cylinder when *Ur* surpasses 15.03.

The principal frequencies in IL direction of cylinder I exhibit a strong concordance with those of the solitary cylinder. However, the results of the other three cylinders are significantly affected. For cylinders II and IV, the mode jump phenomena are more frequently at low reduced velocities. Corresponding to the multiple principal mode responses depicted in Fig. 10, the oscillations in IL direction observed for cylinders II and IV display two distinct and prominent frequency components when *Ur* exceeds 8.77. The high-frequency components, increasing with *Ur*, closely approximate the IL principal frequency of a solitary cylinder. While the magnitude for low-frequency component corresponds to roughly half the magnitude of the high-frequency component. In a prior investigation on FIVs of a flexible cylinder system arranged in a triangular configuration (Ma et al., 2019; Ma et al., 2020), it has been identified that the downstream adjacent cylinders exhibit two prominent frequency components, ascribing wake interference originating from the leading cylinder. The principal frequencies in IL direction of cylinder III exhibit significantly lower values compared to those of the solitary cylinder. Moreover, these principal frequencies even marginally fall below the low-frequency components observed in cylinders II and IV. In contrast to the outcomes from the remaining three upstream cylinders, the principal frequencies in IL direction of cylinder III demonstrate less sensitivity to decreasing velocities. Over a specific range of *Ur*, the principal frequencies remain relatively stable and exhibit slow growth instead of dramatic escalation.

The IL vibration frequencies at measuring positions of the four flexible cylinders for incidence angle 45° are presented in Fig. 14. A prominent frequency of 16.63Hz, which is corresponding to the 5th-order vibration mode, is identified as the principal frequency of cylinder I. In addition to this principal frequency, a minor harmonic component at around 8.25 Hz that approximately matches the CF principal frequency is also observed in Fig. 14(a). Ascribing the influence of added mass, vibration frequencies for the cylinder can experience a slight elevation above the natural frequencies (Han et al., 2018a; Vikestad et al., 2000). In alignment with the outcomes depicted in Fig. 13, cylinders II and IV display two distinct and prominent frequency components in IL oscillation. These two components are relative to the 3rd- and 5th-order vibration modes, respectively. It should be pointed out that the principal frequency refers to the vibration frequency of the principal mode. Competitions between the two components arise in IL direction due to the simultaneous dominance of two vibration modes. Despite the slightly higher RMS value of the modal weights for the 5th-order mode, frequency component associated with this mode might not consistently surpass the frequency component linked to the competing mode at all axial positions. The outcomes of oscillation frequency of cylinder III exhibit a high degree of complexity, attributed to the intricate wake interference caused by the presence of the three leading cylinders. Several wide frequency bands instead of the narrow frequency components are observed for cylinder III. The frequency band between 6.0 Hz and 8.0 Hz takes over the IL vibrations, and this band has dual peaks with the frequency components of 7.27Hz and 7.69Hz. The remaining two frequency bands emerge within the lower frequency range, around 2.5 Hz, and the higher frequency range, approximately 14.5 Hz.

Fig. 15 depicts the max RMS values of displacements of the four flexible cylinders at $\beta = 45°$. The maximum y_{rms}/D values for cylinder I exhibit a high level of concordance with those of the solitary cylinder across the majority of reduced velocities. However, noticeable disparities are observed in the maximum y_{rms}/D values for cylinders II and IV, which can be attributed to three primary factors. Firstly, wake interference arising from the upstream cylinder I plays quite important roles.

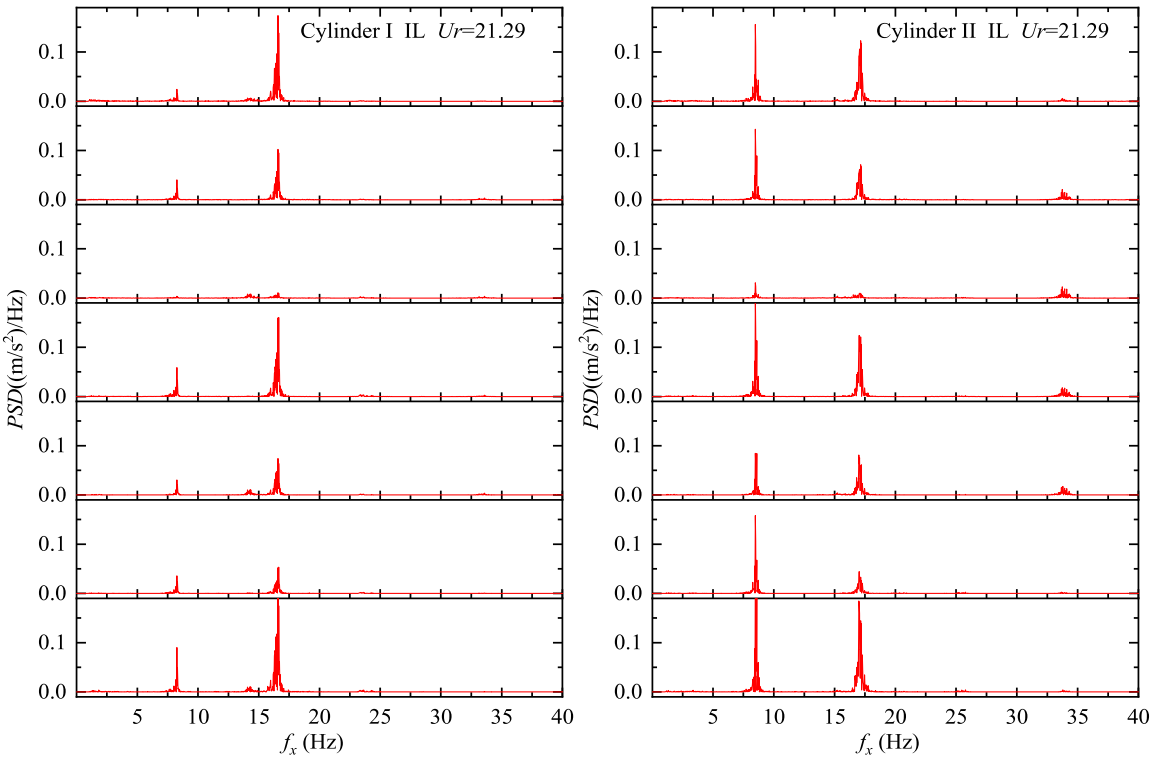

(a) IL vibration frequencies of cylinder I at *Ur*=21.29. (b) IL vibration frequencies of cylinder II at *Ur*=21.29.

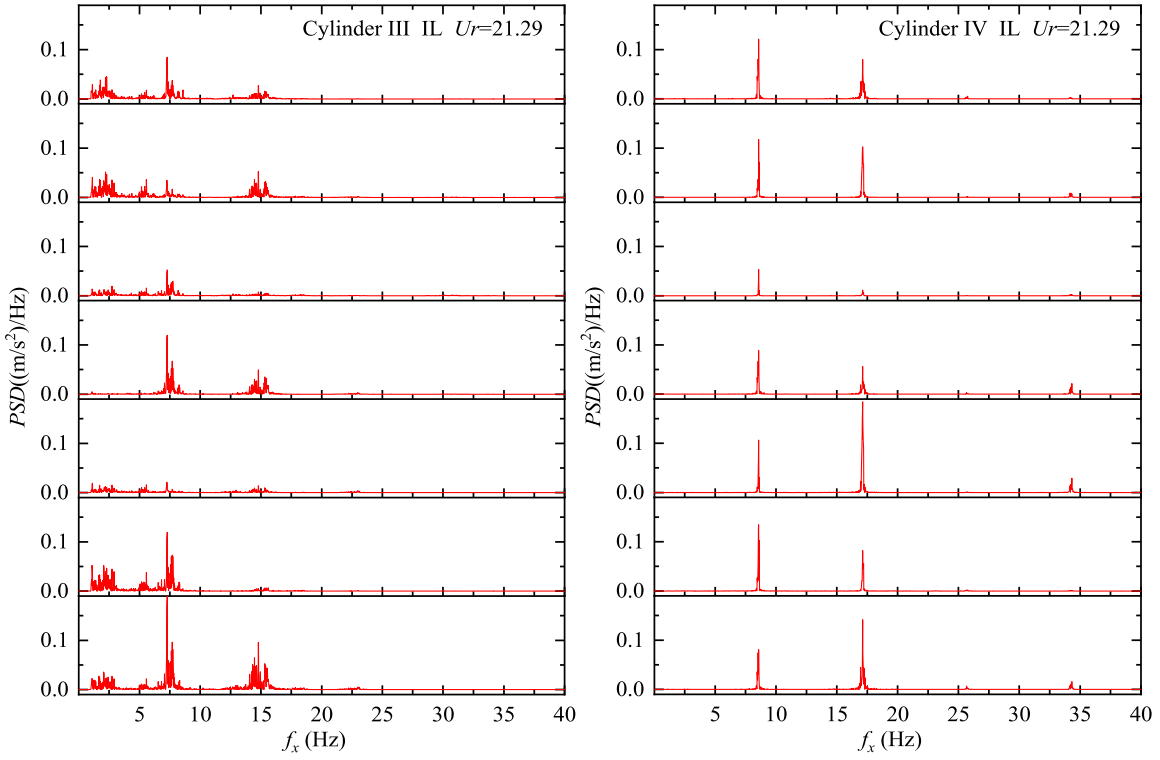

(c) IL vibration frequencies of cylinder III at *Ur*=21.29. (d) IL vibration frequencies of cylinder IV at *Ur*=21.29.

Fig. 14. IL vibration frequencies at measuring positions of the four flexible cylinders for incidence angle 45°.

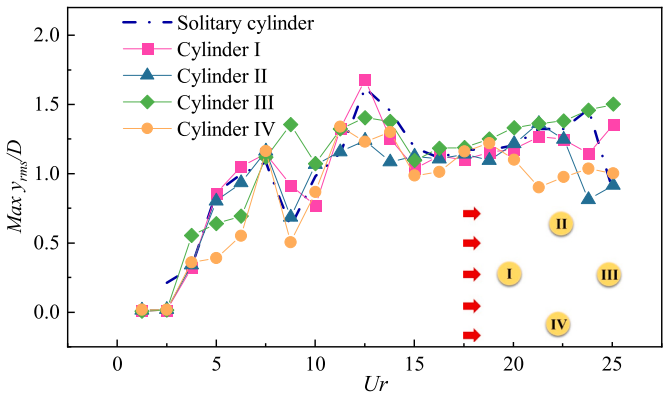

(a) Max RMS of dimensionless displacements in CF direction.

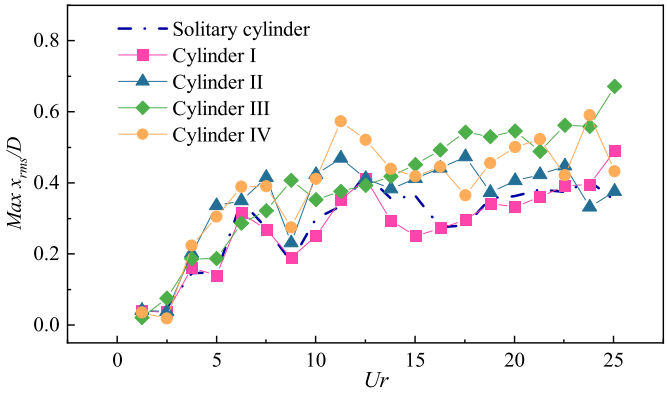

(b) Max RMS of dimensionless displacements in IL direction.

Fig. 15. Max RMS of displacements of the four flexible cylinders when the incidence angle $\beta = 45°$.

Secondly, the proximate effect stemming from their side-by-side configuration contributes to the variation. Lastly, downstream cylinder III further adds to the complexity in the situation. The maximum y_{rms}/D values for cylinders II and IV exhibit a minor reduction compared to those of the solitary cylinder across the majority of reduced velocities, which contradicts findings reported for a two flexible cylinder system (Xu et al., 2018a) and a three flexible cylinder system positioned in the triangular arrangement (Ma et al., 2019). This inconsistency suggests that the presence of cylinder III could disturbs wake flows within the region encompassing the four cylinders, which causes the slight decrease in max y_{rms}/D of cylinders II and IV. Similar to the results of three equilateral-triangular arranged flexible cylinders, the maximum y_{rms}/D of cylinder III attains a higher peak at a greater Ur in comparison to the solitary cylinder. This phenomenon has also been noted for four quadrilateral-arranged rigid cylinders with elastic support (Gao et al., 2019), but continuous increase in CF oscillations of a flexible cylinder is not sustained owing to the activation of higher-order modes.

The maximum y_{rms}/D values for cylinder I are in close proximity to that of the solitary cylinder. However, cylinders II and IV have larger x_{rms}/D than the solitary cylinder in general. Substantial oscillation amplitudes in IL direction of the middle cylinders II and IV are similarly noted in FIV of four quadrilateral-arranged rigid cylinders with elastic support (Gao et al., 2019). The enlargement of IL displacements is closely linked to the principal low-frequency components illustrated in Fig. 14(b) and (c), which has been confirmed in previous study about FIV of three flexible cylinders (Ma et al., 2019). Behaviours exhibited by cylinders II and IV resemble the WIF responses observed in FIVs of a pair of flexible cylinders positioned in the staggered configuration (Xu et al., 2020; Xu et al., 2021b). The amplified IL oscillation amplitudes and the preponderant low-frequency, closely approximating the principal frequency in CF direction, are indicative symbols of WIF. The IL oscillations of cylinders II and IV exhibit two preponderant frequency components. The higher-frequency component closely approximates principal frequency in IL direction of a solitary cylinder, while the lower one is situated near their respective principal frequency in CF direction. As a consequence, behaviours of cylinders II and IV are a composite result of both VIV and WIF. As for cylinder III, its IL oscillations undergo a progressive escalation, with the extreme value of x_{rms}/D reaching 60% above that of the solitary cylinder. The significant IL oscillation amplitudes observed in cylinder III are similarly identified in FIV investigations involving four quadrilateral-arranged rigid cylinders at $\beta = 45°$ (Gao et al., 2019), as well as three flexible cylinders positioned in a triangular configuration (Ma et al., 2019). WIF responses in cylinder III are triggered by the existence of cylinders II and IV, despite the broadband characteristics evident in the spectra as depicted in Fig. 14(c).

Fig. 16 displays the contour plot of dimensionless displacements, axial distribution plot of the RMS displacements, and temporal history curves of displacement at measuring positions of the four flexible cylinders for incidence angle 45°. The reduced velocity of 21.29 is selected to present the high order mode response. For cylinder I, the CF responses are standing waves and the IL responses are a hybrid of standing and traveling wave. The axial distribution plot of RMS displacements exhibits an approximate symmetry and reveals the dominance of the 3rd-order for CF oscillations and the 5th-order for IL oscillations. Reactions of cylinder I more closely resemble VIVs of the solitary cylinder, especially when in comparison to the behaviours of cylinders I and IV in the case of incidence angle 0°. As for cylinders II and IV, their responses in CF and IL directions embody the hybrid features of standing and traveling wave patterns. Because of the wake interference stemming from cylinder I, temporal history curves of displacement at measuring positions reveal the presence of multiple harmonic components. The contour plots of dimensionless displacements in IL direction exhibit some V shapes or inverse V shapes, suggesting a pattern in which the vibrations may shift between the 5th-order and the 3rd-order. For example, axial distribution plots of the RMS displacements display five prominent peaks at a specific time instance. At the subsequent time point, three significant peaks near the middle section of the cylinder along with two less pronounced peaks near the cylinder's ends are observable. The above pattern is reminiscent of the 3rd-order mode vibrations. Cylinder III displays the hybrid features of standing and traveling wave patterns within its oscillations in CF direction, while its oscillations in IL direction are characterized by traveling waves. The oscillations in the two directions exhibit the characteristics of the 3rd-order mode. The temporal history curves of displacement at measuring positions show unstable vibrations containing numerous harmonic components, attributed to the intricate wake interference stemming from the remaining three leading cylinders.

Fig. 17 shows motion trajectories of four cylinders at measuring positions in the case of $\beta = 45°$, and G1 ~G7 are arranged from the uppermost row to the lowest. The time history range of the motion trajectory is during 26s–29s. The motion trajectories of cylinder I at the majority of measuring positions are of a figure-eight shape, which is consist with the outcomes observed for the solitary cylinder undergoing VIV. For cylinders II and IV, the motion trajectories exhibit a slightly more disordered pattern compared to those of a solitary cylinder, attributed to the presence of the two prominent frequency components illustrated in Fig. 14. Figure-eight shape and crescent shape motion trajectories are prevalent across the majority of measuring positions, indicating that the magnitudes of IL frequency are approximately double those of CF frequency. An elliptical motion trajectory, suggesting that the magnitudes of IL frequency are approximately equivalent to those of CF frequency, is also evident at certain measuring positions, such as G6 of cylinder IV. For four quadrilateral-arranged rigid cylinders at $\beta = 45°$ (Gao et al., 2019), figure-eight shape, crescent shape and elliptical shape

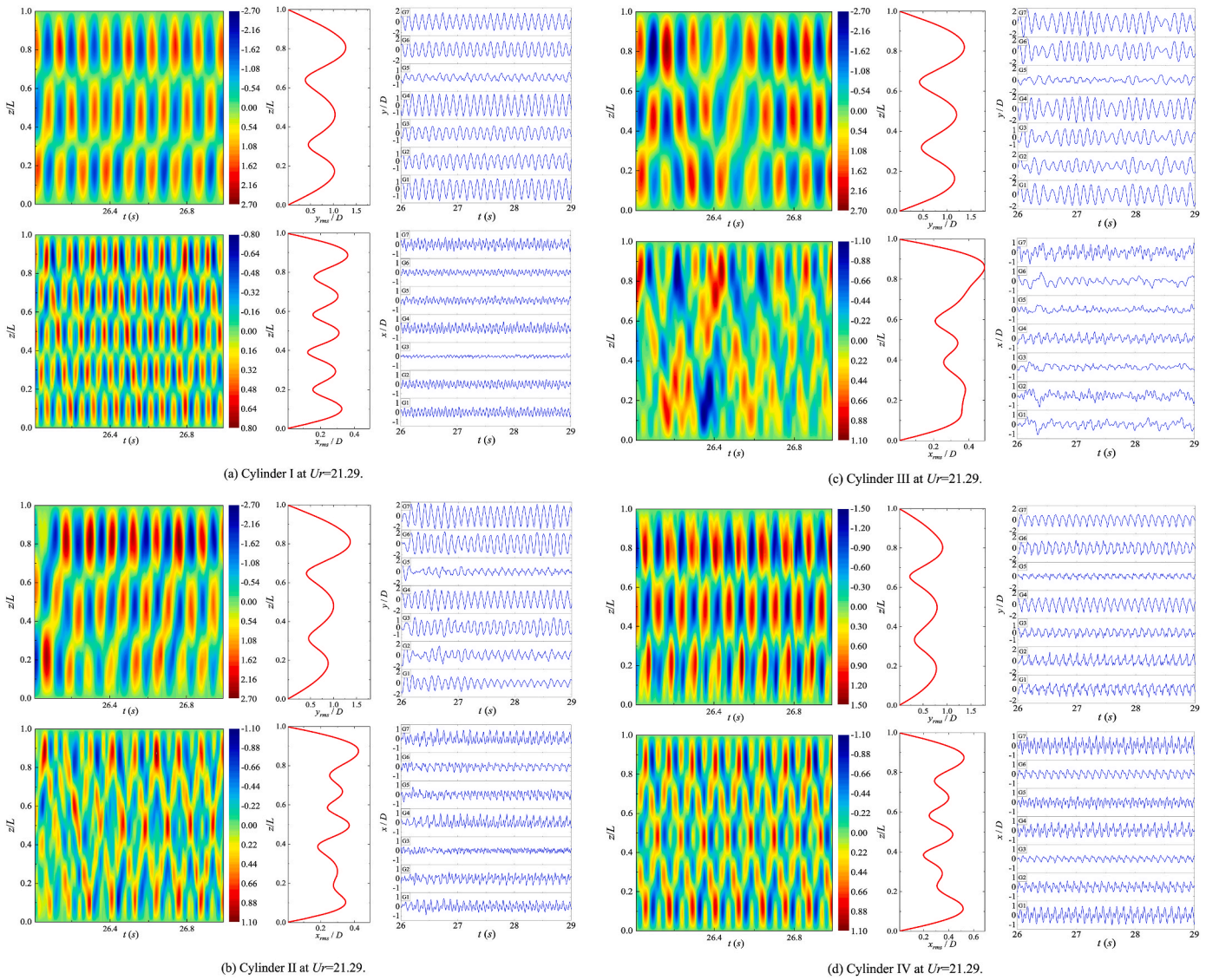

(a) Cylinder I at Ur=21.29.

(c) Cylinder III at Ur=21.29.

(b) Cylinder II at Ur=21.29.

(d) Cylinder IV at Ur=21.29.

Fig. 16. Contour plot of dimensionless displacements, axial distribution plot of the RMS displacements, and temporal history curves of displacement at measuring positions of the four flexible cylinders for incidence angle 45°.

motion trajectories with large IL displacements are also apparent in oscillations of the two middle cylinders. Motion trajectories further shows that the responses of cylinders II and IV result from a combination of a combination of VIV and WIF. Motion trajectories of cylinder III are not repeatable due to the many harmonic components stemming from the intricate wake interference caused by the remaining three leading cylinders. The previous study about FIV of four quadrilateral-arranged rigid cylinders at $\beta = 45^{\circ}$ shows that the vortex emanating from cylinder I consistently collide directly with cylinder III, while the inner vortices generating from cylinders II and IV indirectly disrupt the process of vortex emanating from cylinder III (Gao et al., 2019).

5. Conclusions

Experimental tests were performed to study FIV of four quadrilateral-arranged flexible cylinders. The study encompassed two distinct scenarios, each associated with an incidence angle of 0° and 45°. Through an examination of the dynamic responses, encompassing aspects like the principal vibration modes, response frequencies, response amplitudes and motion trajectories, the following conclusions were drawn.

(1) In the case of incidence angle 0°, the configuration of four quadrilateral-arranged flexible cylinders cannot be simplistically viewed as two sets of tandem cylinders arranged in parallel. The oscillations exhibited by the two upstream cylinders share characteristics observed in a pair of flexible cylinders positioned side-by-side, which is primarily attributed to the proximate effect. The existence of the two downstream cylinders exhibits limited impacts on oscillations of the two upstream cylinders. Nevertheless, behaviours observed for two downstream cylinders exhibit distinctive attributes. Oscillation frequencies in CF direction of the two downstream cylinders are slightly reduced than that of a solitary cylinder, owing to wake interference. The oscillation frequencies in IL direction significantly decrease to the values close to those in CF direction, resulting in the elliptical-shaped motion trajectory. The extreme RMS values of the IL oscillation amplitude for downstream cylinders exceed those of a solitary cylinder by 76% and 71% respectively, which is worth noting in engineering practices.

(2) In the case of incidence angle 45°, reactions observed in upstream cylinder I closely resemble that of a solitary cylinder undergoing VIV. Responses of the pair of middle cylinders II and IV

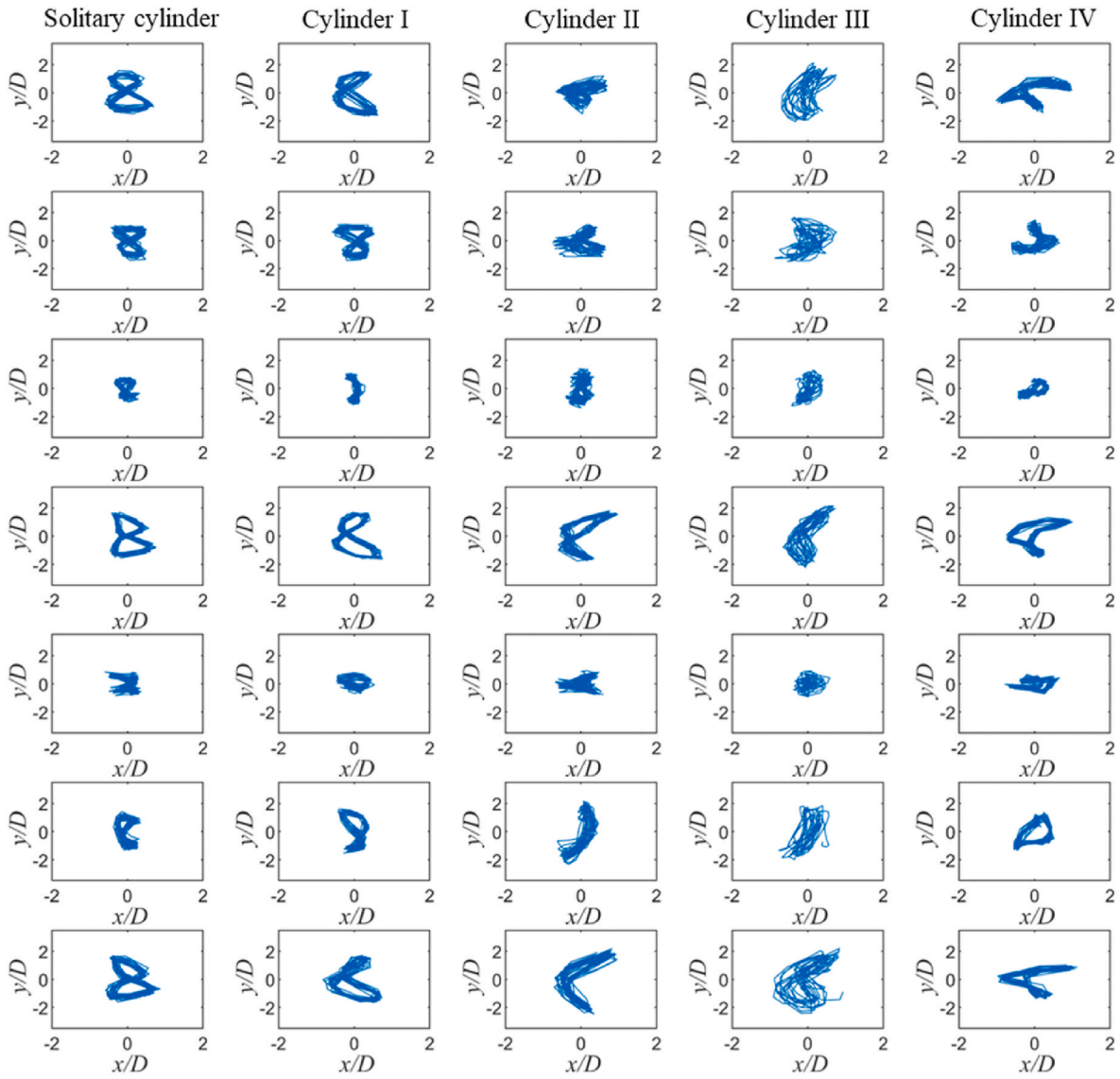

Fig. 17. Motion trajectories of four cylinders at measuring positions in the case of $\beta = 45°$.

encompass a association of VIV and WIF, which is consistent with the FIV behaviours observed in two flexible cylinders positioned in a staggered configuration. Two distinct frequencies stand out in IL direction, with a lower one closely approximating the principal frequency in CF direction. Motion trajectories are figure eight shape and elliptical shape with remarkable IL vibration amplitudes. The extreme RMS values in IL oscillations of downstream cylinder III surpass that of a solitary cylinder by 60% under the intricate wake interference originating from the three upstream cylinders. However, the oscillation frequency is markedly lower than that of a solitary cylinder. The oscillations include many frequency components and the displacement spectra show the broadband feature, which can be responsible for the disordered motion trajectories.

CRediT authorship contribution statement

Yexuan Ma: Conceptualization, Methodology, Supervision, Writing – review & editing. **Zhiyou Song:** Methodology, Investigation, Visualization. **Jingyu Xu:** Investigation, Supervision, Writing – review & editing. **Wanhai Xu:** Conceptualization, Methodology, Investigation, Writing – review & editing.

Declaration of competing interest

All authors of this manuscript have directly participated in the planning, execution, and/or analysis of this study. The contents of this manuscript have not been copyrighted or published previously. The contents of this manuscript are not now under consideration for publication elsewhere. There are no directly related manuscripts or abstracts, published or unpublished, by any authors of this manuscript.

Data availability

Data will be made available on request.

Acknowledgments

This research work was finically supported by National Natural Science Foundation of China (U2106223 and 51979163), China; China Postdoctoral Science Foundation (2023M733588), China; Special Research Assistant Programs Foundation of the Chinese Academy of Sciences (E3XM040201), China.

References

Alam, M.M., Kim, S., 2009. Free vibration of two identical circular cylinders in staggered arrangement. Fluid Dynam. Res. 41, 035507.

Alam, M.M., Moriya, M., Sakamoto, H., 2003. Aerodynamic characteristics of two side-by-side circular cylinders and application of wavelet analysis on the switching phenomenon. J. Fluid Struct. 18, 325–346.

Assi, G.R.S., 2014. Wake-induced Vibration of Tandem and Staggered Cylinders with Two Degrees of Freedom, vol. 50, pp. 340–357.

Assi, G.R.S., Bearman, P.W., Meneghini, J.R., 2010. On the wake-induced vibration of tandem circular cylinders: the vortex interaction excitation mechanism. J. Fluid Mech. 661, 365–401.

Bansal, M.S., Yarusevych, S., 2017. Experimental study of flow through a cluster of three equally spaced cylinders. Exp. Therm. Fluid Sci. 80, 203–217.

Bearman, P.W., Wadcock, A.J., 1973. The interaction between a pair of circular cylinders normal to a stream. J. Fluid Mech. 61, 499–511.

Chaplin, J.R., Bearman, P.W., Huera Huarte, F.J., Pattenden, R.J., 2005. Laboratory measurements of vortex-induced vibrations of a vertical tension riser in a stepped current. J. Fluid Struct. 21, 3–24.

Chen, W., Ji, C., Xu, D., Alam, M.M., 2022. Three-dimensional direct numerical simulations of two interfering side-by-side circular cylinders at intermediate spacing ratios. Appl. Ocean Res. 123, 103162.

Chen, W., Ji, C., Xu, W., Liu, S., Campbell, J., 2015. Response and wake patterns of two side-by-side elastically supported circular cylinders in uniform laminar cross-flow. J. Fluid Struct. 55, 218–236.

Fukushima, H., Yagi, T., Shimoda, T., Noguchi, K., 2021. Wake-induced instabilities of parallel circular cylinders with tandem and staggered arrangements. J. Wind Eng. Ind. Aerod. 215, 104697.

Gao, Y., Yang, K., Zhang, B., Cheng, K., Chen, X., 2019. Numerical investigation on vortex-induced vibrations of four circular cylinders in a square configuration. Ocean. Eng. 175, 223–240.

Griffith, M.D., Lo Jacono, D., Sheridan, J., Leontini, J.S., 2017. Flow-induced vibration of two cylinders in tandem and staggered arrangements. J. Fluid Mech. 833, 98–130.

Gu, Z., Sun, T., 2001. Classification of flow pattern on three circular cylinders in equilateral-triangular arrangements. J. Wind Eng. Ind. Aerod. 89, 553–568.

Haider, B.A., Sohn, C.H., 2022. Effect of degrees of structural freedom on the flow-induced vibrations of isolated and tandem cylindrical structures. Ocean. Eng. 266, 113029.

Han, Q., Ma, Y., Xu, W., Fan, D., Wang, E., 2018a. Hydrodynamic characteristics of an inclined slender flexible cylinder subjected to vortex-induced vibration. Int. J. Mech. Sci. 148, 352–365.

Han, Q., Ma, Y., Xu, W., Zhang, S., 2018b. An experimental study on the hydrodynamic features of two side-by-side flexible cylinders undergoing flow-induced vibrations in a uniform flow. Mar. Struct. 61, 326–342.

Han, Z., Zhou, D., Gui, X., Tu, J., 2013. Numerical study of flow past four square-arranged cylinders using spectral element method. Comput. Fluids 84, 100–112.

Huang, S., Herfjord, K., 2013. Experimental investigation of the forces and motion responses of two interfering VIV circular cylinders at various tandem and staggered positions. Appl. Ocean Res. 43, 264–273.

Huera-Huarte, F.J., Bangash, Z.A., González, L.M., 2016. Multi-mode vortex and wake-induced vibrations of a flexible cylinder in tandem arrangement. J. Fluid Struct. 66, 571–588.

Huera-Huarte, F.J., Bearman, P.W., 2011. Vortex and wake-induced vibrations of a tandem arrangement of two flexible circular cylinders with near wake interference. J. Fluid Struct. 27, 193–211.

Huera-Huarte, F.J., Gharib, M., 2011. Vortex- and wake-induced vibrations of a tandem arrangement of two flexible circular cylinders with far wake interference. J. Fluid Struct. 27, 824–828.

Kareem, A., Kijewski, T., Lu, P.C., 1998. Investigation of interference effects for a group of finite cylinders. J. Wind Eng. Ind. Aerod. 77–78, 503–520.

Khan, H.H., Islam, M.D., Fatt, Y.Y., Janajreh, I., Alam, M.M., 2022. Flow-induced vibration on two tandem cylinders of different diameters and spacing ratios. Ocean. Eng. 258, 111747.

Kim, S., Alam, M.M., 2015. Characteristics and suppression of flow-induced vibrations of two side-by-side circular cylinders. J. Fluid Struct. 54, 629–642.

Kim, S., Alam, M.M., Sakamoto, H., Zhou, Y., 2009. Flow-induced vibrations of two circular cylinders in tandem arrangement. Part 1: characteristics of vibration. J. Wind Eng. Ind. Aerod. 97, 304–311.

Lam, K., Fang, X., 1995. The effect of interference of four equispaced cylinders in cross flow on pressure and force coefficients. J. Fluid Struct. 9, 195–214.

Lam, K., Li, J.Y., Chan, K.T., So, R.M.C., 2003a. Flow pattern and velocity field distribution of cross-flow around four cylinders in a square configuration at a low Reynolds number. J. Fluid Struct. 17, 665–679.

Lam, K., Li, J.Y., So, R.M.C., 2003b. Force coefficients and Strouhal numbers of four cylinders in cross flow. J. Fluid Struct. 18, 305–324.

Lam, K., Lo, S.C., 1992. A visualization study of cross-flow around four cylinders in a square configuration. J. Fluid Struct. 6, 109–131.

Lin, K., Wang, J., Fan, D., Triantafyllou, M.S., 2021. Flow-induced cross-flow vibrations of long flexible cylinder with an upstream wake interference. Phys. Fluids 33, 065104.

Lie, H., Kaasen, K.E., 2006. Modal analysis of measurements from a large-scale VIV model test of a riser in linearly sheared flow. J. Fluid Struct. 22, 557–575.

Ma, Y., Luan, Y., Xu, W., 2020. Hydrodynamic features of three equally spaced, long flexible cylinders undergoing flow-induced vibration. Eur. J. Mech. B-Fluid. 79, 386–400.

Ma, Y., Xu, W., Liu, B., 2019. Dynamic response of three long flexible cylinders subjected to flow-induced vibration (FIV) in an equilateral-triangular configuration. Ocean. Eng. 183, 187–207.

Ma, Y., Xu, W., Pang, T., Wang, Q., Lai, J., 2020. Dynamic characteristics of a slender flexible cylinder excited by concomitant vortex-induced vibration and time-varying axial tension. J. Sound Vib. 485, 115524.

Ma, Y., Xu, W., Zhai, L., Ai, H., 2019. Hydrodynamic characteristics of two tandem flexible cylinders undergoing flow-induced vibration. Ocean. Eng. 193, 106587.

Mousavisani, S., Castro, G., Seyed-Aghazadeh, B., 2022. Experimental investigation on flow-induced vibration of two high mass-ratio flexible cylinders in tandem arrangement. J. Fluid Struct. 113, 103640.

Narváez, G.F., Schettini, E.B., Silvestrini, J.H., 2020. Numerical simulation of flow-induced vibration of two cylinders elastically mounted in tandem by immersed moving boundary method. Appl. Math. Model. 77, 1331–1347.

Nguyen, V., Hong, W., Chan, R., Nguyen, H.H., 2018. Numerical investigation of wake induced vibrations of cylinders in tandem arrangement at subcritical Reynolds numbers. Ocean. Eng. 154, 341–356.

Pouryoussefi, G., Mirzaei, M., Ardekani, M.A., 2009. Experimental investigation of force coefficients for groups of three and four circular cylinders subjected to a cross-flow. Mech. Aerosp. Eng. J. 5, 87–95.

Prasanth, T.K., Mittal, S., 2009. Flow-induced oscillation of two circular cylinders in tandem arrangement at low Re. J. Fluid Struct. 25, 1029–1048.

Sanaati, B., Kato, N., 2014. A study on the proximity interference and synchronization between two side-by-side flexible cylinders. Ocean. Eng. 85, 65–69.

Sayers, A.T., 1990. Vortex shedding from groups of three and four equispaced cylinders situated in a cross flow. J. Wind Eng. Ind. Aerod. 34, 213–221.

Sayers, A.T., 1987. Flow interference between three equispaced cylinders when subjected to a cross flow. J. Wind Eng. Ind. Aerod. 26, 1–19.

Song, J.N., Lu, L., Teng, B., Park, H.I., Tang, G.Q., Wu, H., 2011. Laboratory tests of vortex-induced vibrations of a long flexible riser pipe subjected to uniform flow. Ocean. Eng. 38, 1308–1322.

Sumner, D., 2010. Two circular cylinders in cross-flow: a review. J. Fluid Struct. 26, 849–899.

Sumner, D., Price, S.J., Païdoussis, M.P., 2000. Flow-pattern identification for two staggered circular cylinders in cross-flow. J. Fluid Mech. 411, 263–303.

Tatsuno, M., Amamoto, H., Ishi-i, K., 1998. Effects of interference among three equidistantly arranged cylinders in a uniform flow. Fluid Dynam. Res. 22, 297–315.

Trim, A.D., Braaten, H., Lie, H., Tognarelli, M.A., 2005. Experimental investigation of vortex-induced vibration of long marine risers. J. Fluid Struct. 21, 335–361.

Tu, J., Zhang, Z., Lv, H., Han, Z., Zhou, D., Yang, H., Fu, S., 2020. Influence of the center cylinder on the flow characteristics of four- and five-cylinder arrays at subcritical Reynolds number. Ocean. Eng. 218, 108245.

Vikestad, K., Vandiver, J.K., Larsen, C.M., 2000. Added mass and oscillation frequency for a circular cylinder subjected to vortex-induced vibrations. J. Fluid Struct. 14, 1071–1088.

Wang, E., Xiao, Q., Zhu, Q., Incecik, A., 2017. The effect of spacing on the vortex-induced vibrations of two tandem flexible cylinders. Phys. Fluids 29, 077103.

Wang, E., Xu, W., Yu, Y., Zhou, L., Incecik, A., 2019. Flow-induced vibrations of three and four long flexible cylinders in tandem arrangement: an experimental study. Ocean. Eng. 178, 170–184.

Wang, H., Yu, G., Yang, W., 2013. Numerical study of vortex-induced vibrations of three circular cylinders in equilateral-triangle arrangement. Adv. Mech. Eng. 1–14.

Williamson, C.H.K., 1985. Evolution of a single wake behind a pair of bluff bodies. J. Fluid Mech. 159, 1–18.

Wu, Y.L., 2017. Numerical simulation of flows past multiple cylinders using the hybrid local domain free discretization and immersed boundary method. Ocean. Eng. 141, 477–492.

Xu, F., Xiao, Y.Q., Liu, H.T., Ou, J.P., 2014. Numerical study on vortex-induced vibration of three cylinders in equilateral-triangular arrangements. Lect. Notes Mech. Eng. 8, 391–398.

Xu, W., Cheng, A., Ma, Y., Gao, X., 2018a. Multi-mode flow-induced vibrations of two side-by-side slender flexible cylinders in a uniform flow. Mar. Struct. 57, 219–236.

Xu, W., Ji, C., Sun, H., Ding, W., Bernitsas, M.M., 2019. Flow-induced vibration of two elastically mounted tandem cylinders in cross-flow at subcritical Reynolds numbers. Ocean. Eng. 173, 375–387.

Xu, W., Ma, Y., Cheng, A., Yuan, H., 2018b. Experimental investigation on multi-mode flow-induced vibrations of two long flexible cylinders in a tandem arrangement. Int. J. Mech. Sci. 135, 261–278.

Xu, W., Qin, W., Yu, Y., 2020. Flow-induced vibration of two identical long flexible cylinders in a staggered arrangement. Int. J. Mech. Sci. 180, 105637.

Xu, W., Wu, H., Jia, K., Wang, E., 2021a. Numerical investigation into the effect of spacing on the flow-induced vibrations of two tandem circular cylinders at subcritical Reynolds numbers. Ocean. Eng. 236, 109521.

Xu, W., Zhang, S., Ma, Y., Liu, B., 2021b. Fluid forces acting on three and four long side-by-side flexible cylinders undergoing flow-induced vibration (FIV). Mar. Struct. 75, 102877.

Xu, W., Zhang, S., Ma, Y., Liu, B., Wang, J., 2021c. A study on the FIV hydrodynamic force coefficients of two staggered flexible cylinders via an inverse method. Ocean. Eng. 219, 108272.

Xu, W., Wu, H., Sha, M., Wang, E., 2022a. Numerical study on the flow-induced vibrations of two elastically mounted side-by-side cylinders at subcritical Reynolds numbers. Appl. Ocean Res. 124, 103191.

Xu, W., Wu, H., Song, Z., He, Z., Wang, E., Ge, W., Wang, F., 2022b. Flow-induced vibrations of two staggered cylinders with a moderate spacing and varying incident angles at subcritical Reynolds numbers. Ocean. Eng. 258, 111723.

Xu, W., Zhang, S., Liu, B., Wang, E., Bai, Y., 2018. An experimental study on flow-induced vibration of three and four side-by-side long flexible cylinders. Ocean. Eng. 169, 492–510.
Xu, W., Zhang, Q., Ma, Y., Wang, Y., He, C., Lai, J., 2022. Hydrodynamic characteristics of two side-by-side flexible cylinders with different diameters experiencing flow-induced vibration. Ocean. Eng. 243, 110199.
Yang, Z., Wang, X., Si, J.H., Li, Y., 2020. Flow around three circular cylinders in equilateral-triangular arrangement. Ocean. Eng. 215, 107838.
Zdravkovich, M.M., 1987. The effects of interference between circular cylinders in cross-flow. J. Fluid Struct. 1, 239–261.
Zdravkovich, M.M., 1985. Flow induced oscillations of two interfering circular cylinders. J. Sound Vib. 101, 511–521.
Zheng, S., Zhang, W., Lv, X., 2016. Numerical simulation of cross-flow around three equal diameter cylinders in an equilateral-triangular configuration at low Reynolds numbers. Comput. Fluids 130, 94–108.